Effect of snow cover on pan-Arctic permafrost thermal regimes

Hotaek Park[1*], Alexander N. Fedorov[2,4], Mikhail N. Zheleznyak[2], Pavel Y. Konstantinov[2], John E. Walsh[3]

1 Research and Development Center for Global Change, JAMSTEC, Yokosuka, Japan
2 Melnikov Permafrost Institute, SB RAS, Yakutsk, Russia
3 International Arctic Research Center, University of Alaska Fairbanks, Fairbanks, AK 99775, USA
4 International Center BEST, North-East Federal University, Yakutsk, Russia

* Corresponding Author
e-mail: park@jamstec.go.jp

Abstract

This study quantitatively evaluated how insulation by snow depth (SND) affected the soil thermal regime and permafrost degradation in the pan-Arctic area, and more generally defined the characteristics of soil temperature (T_{SOIL}) and SND from 1901 to 2009. This was achieved through experiments performed with the land surface model CHANGE to assess sensitivity to winter precipitation as well as air temperature. Simulated T_{SOIL}, active layer thickness (ALT), SND, and snow density were generally comparable with *in situ* or satellite observations at large scales and over long periods. Northernmost regions had snow that remained relatively stable and in a thicker state during the past four decades, generating greater increases in T_{SOIL}. Changes in snow cover have led to changes in the thermal state of the underlying soil, which is strongly dependent on both the magnitude and the timing of changes in snowfall. Simulations of the period 2001–2009 revealed significant differences in the extent of near-surface permafrost, reflecting differences in the model's treatment of meteorology and the soil bottom boundary. Permafrost loss was greater when SND increased in autumn rather than in winter, due to insulation of the soil resulting from early cooling. Simulations revealed that T_{SOIL} tended to increase over most of the pan-Arctic from 1901 to 2009, and that this increase was significant in northern regions, especially in northeastern Siberia where SND is responsible for 50% or more of the changes in T_{SOIL} at a depth of 3.6 m. In the same region, ALT also increased at a rate of approximately 2.3 cm per decade. The most sensitive response of ALT to changes in SND appeared in the southern boundary regions of permafrost, in contrast to permafrost temperatures within the 60°N–80°N region, which were more sensitive to changes in snow cover. Finally, our model suggests that snow cover contributes to the warming of permafrost in northern regions and could play a more important role under conditions of future Arctic warming.

Keywords: Active layer thickness, Arctic climate, land surface model, permafrost extent, snow depth, soil temperature.

Introduction

Permafrost and snow cover are key components of the Arctic system because of their influences on energy, water, and carbon cycles (e.g., Peterson et al. 2002; Hinzman et al. 2005; Schuur et al. 2009), and their links to global climate. The two components maintain an interactive relationship with each other, which is largely unidirectional and highly seasonal. Snow falls only during the cold winter season. It affects the thermal regime of the permafrost in the winter, and that effect persists into the following summer. Snow also affects the hydrologic conditions during the melt period. An improved understanding of the relationships between snow and permafrost under present-day climate conditions is an important challenge for Arctic and global climate research.

Permafrost is vulnerable to warming temperatures. In recent decades, studies have reported evidence of permafrost degradation and increases in the active layer thickness (ALT; Callaghan et al. 2011; IPCC 2014). Simulations have indicated that the extent of permafrost in the terrestrial Arctic has decreased by about 3–5 million km^2 during the twentieth century (Lawrence et al. 2012; Burke et al. 2013). Other studies have identified increases in the ALT in Russia (Frauenfeld et al. 2004) and North America (Smith et al. 2010), as well as at some sites of the Circumpolar Active Layer Monitoring (CALM) network (Nelson 2004). Models have also simulated deeper ALTs at watershed or continental scales (Oelke et al. 2004; Zhang et al. 2005; Koven et al. 2011; Burke et al. 2013; Park et al. 2013a). However, ground warming does not always respond linearly to surface warming. Moreover, the ALT on the North Slope of Alaska has remained relatively stable, with no changes observed from 1995 to 2008 despite increased air temperatures (Shiklomanov et al. 2010). A similar trend was observed in the northern Mackenzie region, with some decreases in ALT reported since 1998 (Burn and Kokelj 2009; Smith et al. 2009). Stationary or decreasing permafrost temperatures have also been observed in western Canada (Smith et al. 2010) and Alaska (Osterkamp 2007) during the last decade. Surface air temperature (SAT) has increased over most of the terrestrial Arctic during the last decade (Bekryaev et al. 2010). In North America, the differences in soil warming changes relative to rising air temperature suggest the effects of other factors on the ground thermal state. A process-based model has successfully simulated the negative anomaly of ALT in the Mackenzie and Yukon watersheds since 1990 and has highlighted the effects of decreases in both snow depth

(SND) and soil moisture (Park et al. 2013a).

Snow is an effective insulator, resulting in a thermal offset between air and soil. Insulation by snow may be more significant in colder northern regions, where T_{SOIL} is strongly dependent on the thermal regimes created during the snow season. Previous studies, both observational and model-based, have identified regionally large variations in snow cover, with SND tending to increase in northeastern Siberia despite climate warming (Bulygina et al. 2009; Park et al. 2011b), whereas most areas of North America displayed negative SND trends (Schindler and Donahue 2006; Park et al. 2011b). Among the regionally varying trends in SND, significant increases have been identified mainly in coastal regions rather than in interior areas (Park et al. 2013b). The decline in Arctic sea ice cover may be associated with increases in SND over northern regions (Ghatak et al. 2010; Cohen et al. 2012; Park et al. 2013b). However, a data-based analysis has revealed increased poleward atmospheric moisture transport (Zhang et al. 2013), implying higher precipitation and therefore increases in SND in the Arctic. Permafrost temperatures in northern regions have tended to increase, which is consistent with the regional trend in SND (Callaghan et al. 2011). The magnitude of permafrost warming varies regionally, but typically ranges from 0.5ºC to 2ºC at a depth of zero annual amplitude (Osterkamp 2007; Oberman 2008; Romanovsky et al. 2010). Increased permafrost temperatures are not attributable solely to changes in snow cover because winter air temperatures in the northern Arctic have increased significantly during recent decades (Bekryaev et al. 2010). Under this air warming, the increased SND could further amplify permafrost warming. Taken together, this series of studies suggests that changes in snow cover may have played a yet-to-be-quantified role in the regional increases in permafrost temperature.

The North Slope of Alaska, characterized by tundra vegetation, is a region that is particularly susceptible to the influence of snow on permafrost. Permafrost temperatures in some areas across the North Slope of Alaska increased by 2ºC–4ºC from 1910 to 1950 (Lachenbruch and Marshall 1986). These increases were beyond the scope that could be explained by changes in the air temperature during the same period. There was a trend toward increased snowfall during the cold seasons, thereby warming the permafrost (Zhang and Osterkamp 1993). The effect of snow insulation on increased T_{SOIL} was also observed at Irkutsk, Russia, a generally forested (taiga) region in which the ground is seasonally frozen (Zhang et al. 2001). Zhang and Stamnes (1998)

conducted a modeling experiment and then tested an alternate hypothesis that changes in seasonal snow cover affect the thermal regimes of the active layer and permafrost less than changes in mean annual air temperature in northern Alaska. These different findings are not surprising because variations in the temperature of the permafrost might be related to regional and local factors (e.g., vegetation, topography). Variations in permafrost temperature have exhibited considerable heterogeneity during recent decades. While patterns are generally consistent with trends or variations of air temperature and SND (Zhang et al. 2001; Stieglitz et al. 2003; Osterkamp 2007), snow cover also appears to affect permafrost temperature.

Few studies have assessed the relative contribution of snow to changes in permafrost temperatures. Using a model, Lawrence and Slater (2010) found that during the latter half of the twentieth century, variations in snow cover could account for more than 50% of the total T_{SOIL} variations at a depth of 1 m in the Arctic. Modeling results for Barrow, for the period 1977–1998, revealed that about one-half of the permafrost warming at a depth of 20 m was attributable to the effect of increased SND, while the remainder was the result of increased air temperature (Stieglitz et al. 2003).

The lack of observation-based assessments is likely a consequence of the lack of widespread long-term observations of T_{SOIL} and related climatic variables. Existing borehole data provide some insights into the changes and trends of permafrost temperatures in response to climate warming. However, observations are very sparse and historically short, creating limitations in understanding current permafrost temperatures in the context of long-term trends, as well as in assessing the degree of permafrost degradation.

Future global warming is expected to exacerbate the changes in snowfall trends during the twenty-first century. The models used in the Coupled Model Intercomparison Project (CMIP3) projected that mean winter snowfall rates by the year 2100 will increase by 15%–45% and that the snow season will shorten across most of the Arctic region (Meehl et al. 2007; Callaghan et al. 2011). The competing processes of increasing snowfall and changes in the length of the snow season could yield complex changes in T_{SOIL}, which will be linked to other processes in the Arctic. In turn, changes in environmental processes in the Arctic are likely to be linked to global changes. For example, permafrost warming has a strong influence on hydrological and biogeochemical processes. Thus, the quantification of the relative effects of snow versus

145 air temperature on T_{SOIL} trends is more important in the context of future regional and
146 global changes.
147 The main objective of this study was to quantitatively evaluate the influences
148 of snow cover on large scale and long-term changes in T_{SOIL}. A process-based land
149 surface model (coupled hydrological and biogeochemical model; CHANGE) was
150 applied over terrestrial regions of the Arctic for the period 1901–2009, with several
151 experimental designs that incorporated different climatic forcing. We not only identified
152 regions in which T_{SOIL} is sensitive to changes in snow cover, but we also defined the
153 spatially varying characteristics of both the soil thermal regime and snow cover
154 simulated for the present-day climate. Additionally, simulated T_{SOIL} and snow values
155 were compared to *in situ* observations. The T_{SOIL} evaluation was confined to soil depths
156 of 3.6 m and greater, in which the influences of latent heat on temperature are not large.
157
158 2. Model, Data, and Methods
159 2.1 Land surface model, CHANGE
160 CHANGE (Park et al. 2011a) is a state-of-the-art process-based model that
161 calculates heat, water, and carbon fluxes in the atmosphere–land system as well as soil
162 thermal and hydrologic states, including an explicit treatment of soil freeze/thaw phase
163 changes, and stomatal physiology and photosynthesis. The carbon absorbed through
164 photosynthesis is partitioned into leaf, stem, root, and soil, which are intertwined with
165 land surface processes. The coupling of the dynamic vegetation model in CHANGE
166 facilitates the integration of interactions and feedbacks in the land system and climate. A
167 notable feature of CHANGE is its improved representation of permafrost dynamics,
168 which has been achieved through the extension of soil depth to 50.5 m to explicitly
169 capture thermal inertia in deep ground. Zero heat flux is prescribed as the lower
170 condition. The heat flux into the soil–snow is obtained by solving an energy balance
171 equation and is used as the upper boundary condition for the solution of the heat
172 conduction. CHANGE numerically solves the heat conduction equation, including soil
173 water phase changes, to simulate heat conduction between soil layers. Solving the
174 equation requires soil heat conductivity and capacity, which are determined as functions
175 of the liquid and ice content, T_{SOIL}, and the vertically heterogeneous soil texture.
176 The model also includes the influence of soil organic matter (SOM) on soil
177 thermal and hydraulic properties, based on the parameterization by Lawrence and Slater

178 (2008). The parameters vary temporally, depending on the amount of simulated soil
179 organic carbon. CHANGE is run with an active terrestrial carbon cycle with the three
180 prognostic litter and SOM pools (i.e., labile, cellulose/hemicellulose, and remaining
181 mass). The transfer of decomposed materials is structured as a converging cascade that
182 flows from the upstream to the downstream pool (Thornton and Rosenbloom 2005). The
183 total soil carbon stored within the SOM pools is used for calculating the vertical profile
184 at every time step. The model assumes that soil carbon is distributed within the soil
185 depth (1.5 m) according to a typical soil carbon profile. The carbon content in boreal
186 and polar soils is concentrated toward the surface, and the carbon density in any
187 individual soil layer does not exceed the bulk density of peat ($\rho_{sc,max}$ = 130 kg m^{-3};
188 Lawrence and Slater 2008). The soil carbon or organic fraction for a particular soil layer
189 ($f_{sc,i}$) is defined as
190
191 $$f_{sc,i} = r_{sc,i} / r_{sc,max}, \quad (1)$$
192
193 where $\rho_{sc,i}$ is the soil carbon density for soil layer i.
194 The soil thermal and hydraulic properties were parameterized as a weighted
195 combination of the separate mineral soil and soil organics (Lawrence and Slater 2008;
196 Park et al. 2011a). Further details on parameterizations of soil thermal properties are
197 described in this section. SOM affects the soil thermal regime significantly because it
198 has lower soil thermal conductivity and a relatively high heat capacity. The soil thermal
199 conductivity (λ_i) becomes
200
201 $$/_i = K_{e,i} /_{sat,i} + (1 - K_{e,i}) /_{dry,i}. \quad (2)$$
202
203 The thermal conductivity is calculated as a combination of the saturated ($\lambda_{sat,i}$) and dry
204 ($\lambda_{dry,i}$) thermal conductivities, weighted by a normalized thermal conductivity (K_e, the
205 Kersten number, which is a function of the degree of saturation and phase of water). The
206 saturated thermal conductivity is
207
208 $$/_{sat,i} = /_{s,i}^{1-q_{sat,i}} /_{liq}^{q_{sat,i}} /_{ice}^{q_{sat,i}-q_{liq,i}}, \quad (3)$$
209

where λ_{liq} and λ_{ice} are the liquid water and ice thermal conductivities, respectively, θ_{sat} and θ_{liq} are the volumetric water content at saturation and volumetric liquid water content, respectively, and $\lambda_{s,i}$ is the solid thermal conductivity combined with the organic soil. The latter is calculated as

$$/_{s,i} = (1 - f_{sc,i})/_{s,\min,i} + f_{sc,i}/_{s,sc}, \quad (4)$$

where $\lambda_{s,sc}$ is the thermal conductivity of organic soil solids (0.25 W m^{-1} K^{-1}) and $\lambda_{s,\min,i}$ is the empirically derived thermal conductivity of solid mineral soil.

The soil heat capacity is given by

$$c_i = c_{s,i}(1 - q_{sat,i}) + w_{liq,i}C_{liq} + w_{ice,i}C_{ice}, \quad (5)$$

where w_{liq} and w_{ice} are the liquid water and ice content, respectively, for the soil layer, C_{liq} and C_{ice} are specific heat capacities of liquid water and ice, respectively, and $c_{s,i}$ is the heat capacity of solid soil, which is the combination of mineral ($c_{s,\min,i}$) and organic soil ($c_{s,sc}$). The latter is given by

$$c_{s,i} = (1 - f_{sc,i})c_{s,\min,i} + f_{sc,i}c_{s,sc}, \quad (6)$$

where $c_{s,sc}$ has a value of 2.5×10^6 J m^{-3} K^{-1}.

The CHANGE model adopts a two-layer energy and mass balance approach to simulate snow accumulation and snowmelt at the surface. The energy balance includes snowmelt, refreezing, and changes in the snowpack heat content. The mass balance components represent snow accumulation/ablation, changes in the snow water equivalent, and water yield from the snowpack. The snowpack compacts with snowfall and time, which increases gravitational settling and the densification of the snowpack. Therefore, compaction represents the sum of metamorphism and overburden, affecting snow density. SND can be estimated from the simulated snow density and snow water equivalent. The model includes the process of canopy snow interception because when a vegetation canopy is present, it intercepts part of the snowfall.

In the radiation balance calculation, shortwave radiation is divided into direct-beam and diffuse radiation because the canopy and soil have different spectral

properties for individual spectral bands. The albedo of the canopy, soil, and snow is also calculated using a two-stream approximation method, in which the ground albedo is determined by weighting the soil and snow albedos. Evapotranspiration is calculated as the sum of partitioned transpiration, interception, and soil evaporation. Transpiration is largely dependent on variations in the leaf area index and root profile, and their spatiotemporal variations are simulated by the model at each time step. Park et al. (2011a) provide a full description of CHANGE.

2.2 Meteorological forcing data

A European Union project (Water and Global Change; WATCH) has yielded a global gridded meteorological dataset at a $0.5^{o} \times 0.5^{o}$ scale (Weedon et al. 2011), which allows global simulation of land surface processes at 3-h time steps covering the period 1901–2001 (WFD). The generation of this dataset was described in detail by Weedon et al. (2011), so we only provide the major characteristics here. During the first processing step, ERA-40 data were interpolated at a half-degree grid resolution, which is consistent with the land–sea mask defined by the Climatic Research Unit (CRU, http://www.cru.uea.ac.uk/data). Then, elevation corrections were applied to the grid-interpolated components (e.g., temperature, surface pressure, specific humidity, and downward longwave radiation). The 2-m temperatures in ERA-40 are known to lack some climatic trends and to exhibit an overall bias. Therefore, the gridded monthly CRU temperatures (CRU TS2.1) were used for this bias correction. However, the CRU temperatures also include some inhomogeneities that, at particular sites and for some single month outliers, introduce steplike offsets in the values spanning several years; these inhomogeneities were removed. Next, the CRU data were used to correct the monthly bias in temperature and averaged monthly diurnal temperature ranges. The relative humidity was grid-interpolated on the basis of the original ERA-40 temperature, pressure, and specific humidity, and the resulting values were used to calculate specific humidity with elevation- and bias-corrected temperature and pressure. Shortwave downward radiation was also monthly bias-corrected using CRU cloud cover data and the local linear correlation between monthly average ERA-40 cloud cover and downward shortwave radiation. Additionally, an atmospheric aerosol correction was added to the corrected shortwave downward radiation.

The precipitation data for WATCH were generated over six steps using two

datasets: the Global Precipitation Climatology Centre full product (GPCCv4) and CRU TS2.1 (Weedon et al. 2011). GPCCv4 provides more station coverage than CRU data, particularly at high latitudes and for the end of the twentieth century. Therefore, the GPCCv4 was used to correct monthly ERA-40 precipitation totals. ERA-40 precipitation tends to depict too many wet days in the tropics; thus, the monthly number of precipitation days was adjusted to be consistent with the CRU data. These monthly corrections increase precipitation data for some months and a small number of grid boxes, in which the precipitation rates of ERA-40 are close to zero. The corrected precipitation data are reassigned into rainfall and snowfall at each time step and grid box using the original ratio determined from ERA-40 data. The subsequent correction for the precipitation gauge undercatch uses the method of Adam and Lettenmaier (2003).

Because the dataset begins in 1958, ERA-40 data are not available for the first half of the twentieth century. Based on the same data generation process described above, this gap was filled by a random ordering of ERA-40 years from 1958 to 2001. The extraction order excluded replacement by the same years and also assigned leap years (Weedon et al. 2011). This selection approach basically introduces the statistical properties (temporally and spatially) of the ERA-40 period. The procedure also guarantees the same autocorrelation characteristics and the same covariance relationships between variables as during the ERA-40 interval. However, the timing of particular weather events was not correct for the period of 1901–1957 at any location (Weedon et al. 2011).

The WATCH project used 4D-var reanalysis based on ERA-Interim for the period 1979–2009, which provides another forcing dataset (WFDEI). WFDEI used the same interpolation methods as WFD, but used both the air temperature of CRU TS3.1/TS3.101 and the precipitation of GPCCv5 for monthly bias corrections. The differences in the data used for bias corrections and baselines can yield different characteristics between WFD and WFDEI for some variables within the overlap interval (1979–2001). We compared the spatiotemporal distribution and the absolute value of air temperature and precipitation between WFD and WFDEI for the overlap interval and found differences in the absolute values of the variables, although these differences were small and displayed similar distributions. Based on this simple comparison, data for the period 2002–2009 within WFDEI were combined with the period 1901–2001

from WFD and used for simulations with CHANGE.

2.3 Simulations

The forcing data for 1901–2009 were used to drive CHANGE simulations over the land area poleward of 45°N. The land cover was static for the present-day distribution, while the vegetation phenology was prognostic depending on the carbon and nitrogen fluxes. CHANGE used soil texture information in terms of the fractions of sand, silt, and clay derived from the IGBP SoilData System. These fractions were used to estimate soil thermal conductivity, heat capacity, and hydraulic conductivity, in combination with soil organic matter simulated by CHANGE at every time step. The atmospheric CO_2 concentration was set to be time-varying. Simulations were run with a 3-h time step and spun-up by repeatedly simulating the first 20 years until the soil carbon reached a stable state over a minimum of 1800 years. These procedures were applied equally in all experiments performed during this study.

Different sets of numerical experiments were designed to diagnose how changes in snow cover affect the century-scale evolution of Arctic T_{SOIL}. The experiments were based on nine scenarios, including a control run (CTRL) that used the original forcing set (Table 1). Our main objective was to evaluate the quantitative influence of seasonal snow cover on the soil thermal regime because the seasonal variability of snow cover yields different magnitudes of the insulation effect and hence different T_{SOIL} (Zhang 2005). While snowfall may not necessarily translate to snow on the ground (water equivalent, depth, duration), ongoing climate change in the Arctic could force changes in the snow regime. For experimental purposes, snowfall was either increased or decreased by 30% from the amounts projected in the CTRL. The changes were made individually for three different periods: October–December, December–February, and October–February.

Air temperature is a critical variable for T_{SOIL}, as well as for variations of snow cover. SAT can either amplify or offset the effects of snow insulation on the soil thermal regime. To assess the responses of T_{SOIL} to the combination of the modified SAT and SND during the October–February period of snowfall modification, we subjectively selected two periods, 1911–1930 and 1991–2009, as our baselines because they were the coldest and warmest periods, respectively, in the CTRL experiment. The use of baselines maintained constant rates of climatological mean monthly SAT

throughout the simulation period by scaling the SAT of the forcing data (Lawrence and Slater 2010), SAT(y,m,t), at every time step (t) according to

$$\mathrm{SAT}_{\mathrm{const}}\left(y,m,t\right)=\left[\frac{\mathrm{SAT}_{\mathrm{BASLN}}\left(m\right)}{\mathrm{SAT}\left(y,m\right)}\right]\mathrm{SAT}\left(y,m,t\right), \quad (7)$$

where y is the year, m is the month, $\mathrm{SAT}_{\mathrm{BASLN}}(m)$ is the monthly climatological mean for the baseline SAT (1911–1930 or 1991–2009), and SAT(y,m) is the mean monthly SAT for a particular year and month. Different T_{SOIL} values were set for individual experiments relative to the CTRL to evaluate the magnitude of snow cover affecting T_{SOIL}. To reduce any remaining dependence on initial conditions, the treatments described above were applied from the final 20 years of the spin-up.

2.4 Datasets for model validation

Daily SND data over the pan-Arctic region were obtained from the European Climate Assessment and Dataset (ECAD), the Russian Research Institute of Hydrometeorological Information–World Data Center (RIHMI-WDC) (Bulygina et al. 2009), the National Climate Data and Information Archive of Environment Canada (Brown 2000), and the Global Historical Climatology Network (GHCN). From these four datasets, we selected approximately 2400 stations that were located poleward of 45°N and had consecutive winter data (December–February; DJF) for periods longer than 15 years. The European Space Agency (ESA) provides a global snow water equivalent (SWE) product, GlobSnow (Takala et al. 2009), from 1978 to the present, which is available on an EASE-Grid at a 25-km resolution. The GlobSnow dataset is produced by combining a satellite-based microwave radiometer and ground-based weather station data.

Russian meteorological stations measure snow density through routine snow surveys across the former Soviet Union (USSR). The survey is performed throughout the cold season (every 10 days) and during snowmelt (every 5 days). Snow density data are available for 517 stations in RIHMI-WDC, from 1966 to the present. The National Snow and Ice Data Center (NSIDC) also archived snow density data at 1319 stations over the former USSR during the period 1966–2000. Snow density, merged with the two datasets, was used in model validation for 1966–2009. Data that exceeded the range

of 0–0.6 g cm^{-3} were excluded from analysis (Zhong et al. 2014).

For permafrost monitoring, borehole sites established across the former Soviet Union provided ground temperature measurements. The boreholes themselves vary in depth: some are more than 100 m deep, but most are less than 30 m deep. Although most boreholes are no longer operational, they provide a valuable snapshot of permafrost temperatures, mainly from the 1940s to the 1970s. The majority of their data are still unpublished. We mined this data and produced a database of historical borehole temperatures across the former Soviet Union. This was useful for determining the permafrost thermal state prior to 1980 and for model evaluation.

Starting in the 1970s and 1980s, some borehole sites were also installed in the Sakha Republic, Russia, to monitor permafrost temperatures, and equipped with semiconducting temperature sensors (thermistors; MMT-1 or MMT-4), commonly used in permafrost geothermal studies in Russia. The number and depths of thermistors differed between sites, but all sites measured temperature at one common depth among the three borehole depths: 10, 15, and 20 m. During the initial period, measurements were made regularly or irregularly, and varying from annually to monthly depending on location. The accuracy of these measurements using calibrated thermistors was typically equal to or better than 0.1ºC. Since 2000, the boreholes have been equipped with temperature data-loggers (HOBO U-12-008) and TMC-HD temperature sensors with an accuracy of 0.1ºC or better. The temporal resolution of these measurements is typically 3 h. Detailed measurements are reported in Konstantinov (2009) and Zheleznyak (2011). Previously published borehole data measured in permafrost regions in Russia were also used for model validation (Murzin and Rusakov 1996; Pavlov and Moskalenko 2001; Oberman 2007, 2008; Sergueev et al. 2007; Malkova 2008; Skryabin et al. 2008; Vasiliev et al. 2008; Moskalenko 2009; Drozdov et al. 2010, 2012; Skryabin and Varlamov 2012; Boike et al. 2013).

During the late 1970s and early 1980s, numerous borehole sites were installed, mainly in Alaska (Osterkamp 2008) and western Canada (Smith et al. 2010). Additional sites have been established in the pan-Arctic region during recent decades, and particularly during the International Polar Year (IPY). These monitoring sites contribute to the Global Terrestrial Network for Permafrost (GTN-P), which is collecting long-term borehole data from Canada and Alaska, and provides a snapshot of permafrost temperatures obtained during the IPY campaign. Permafrost temperatures

observed in a north–south transect along the Alaskan oil pipeline were obtained from the National Snow and Ice Data Center (NSIDC); these data are available to the year 2003, with different start years for individual sites (Osterkamp 2008).

3. Results

3.1 Comparison of observations versus simulations

3.1.1 Snow cover characteristics

Snow is an effective insulator that limits communication between the atmosphere and ground. If the simulated SND contains systematic errors relative to observations, the influence would directly affect T_{SOIL}. Therefore, the model results were validated against observations. A previous study verified that the CHANGE model simulated the general characteristics of SND at selected stations in the pan-Arctic region (Park et al. 2011b). Here we extended the validation to include large-scale comparisons of simulated winter snow cover against observations. Figure 1 presents the decadal anomalies of snow cover during 2001–2009 (relative to 1991–2000), when air temperatures were in a warming phase (Bekryaev et al. 2010). The period 1991–2009 was selected because GlobSnow provides a full dataset for winter SWE during this period. The simulated SND over the Eurasian continent revealed contrasting anomalies, which were positive in the east and negative in the west (Figure 1c). Although local variations appeared, a similar general pattern of anomalies also appeared in observations from the meteorological stations (Figure 1a) as well as in the SWE derived from satellite measurements (Figure 1b). Other observation- and model-based studies have reported increases in SND in northeastern Siberia (Bulygina et al. 2009; Park et al. 2011b, 2013b). While detailed comparisons of simulated snow against observations were impossible due to the different spatial resolution, the snow simulated for Eurasia displayed spatial variations that were visually consistent with observations.

In North America, meteorological stations are very sparse, particularly in northern Canada. In Canada, the primary snow-observing network began in the late 1980s, but station closures increased rapidly after 2000 (personal communication with R. Brown). The sparse network of meteorological stations is likely to affect SWE estimated by satellite observations because GlobSnow uses ground observations to estimate SWE. In northeastern Canada, simulated SWE significantly disagreed with the spatial pattern based on observational estimates. However, there was better agreement

between simulated and observed patterns in western North America, where there are more stations than in the east, and where a decrease in SND has already been identified (Schindler and Donahue 2006). The decrease of snow cover in this region resulted in soil drought and therefore shallower ALTs (Park et al. 2013a).

Figure 2 compares interannual anomalies in observed and simulated winter SNDs on the pan-Arctic scale. The anomalies are relative to the 1971–2000 means. To minimize the effect of spatially inhomogeneous data coverage on the anomalies, we used a technique similar to the climate anomaly method (Jones et al. 1999; Bekryaev et al. 2010). In this method, the pan-Arctic area is divided into boxes with a scale of 10º latitude and 20º longitude. The anomalous time series of SND for either stations or grid cells within each box were averaged, and the resulting averaged time series of each box were averaged to provide a single time-series at the pan-Arctic scale. Large differences appeared in the anomalous time-series when observed, and simulated results were compared for the period 1901–1960. These differences are likely attributable to the small number of available observation stations during this period. For example, SND for 1901–1935 was determined from values taken at only a few specific stations in Russia. Since 1960, the anomalies of the observation and simulation generally display a similar time series (r = 0.38, $P <$ 0.007). SND has tended to remain at relatively high levels for the past four decades, during which time the SAT has increased (Bekryaev et al. 2010).

The records of snow density from each station or grid pixel were reduced to monthly anomalies relative to 1971–2000. Annual anomalies of winter snow density were averaged when two monthly anomalous values for January to March were available. The averaged anomalies of each station or grid pixel were in turn averaged for a Russian subregion (55°N–70°N, 40°E–140°E) using the same method adopted in Figure 2. Figure 3 compares interannual anomalies between observed and simulated snow densities. The model generally captured the interannual variability of the observations, with a high correlation (r = 0.55, $P <$ 0.0002). However, differences were noted between the two anomalous values since 2000, in which the observed snow density showed a significant decrease. The observation indicated a decreasing trend for the period 1966–2009 (r = 0.29, $P <$ 0.06), in contrast with the increasing trend in the simulation (r = 0.33, $P <$ 0.03). Zhong et al. (2014) also reported decreasing trends in snow density across the former USSR for the period 1966–2008. Russian

meteorological stations are sparse in northernmost regions (see Figure 4 of Zhong et al. 2014). Meanwhile, the model simulated higher increases in SND in the same regions in the 2000s (Figure 6b). These geographical differences likely affect the different trends of snow density. Large differences appeared between simulations and observations in SND and SWE in the region and period for which few meteorological stations were available. In general, few long-term observations are available for northern regions due to the low density of meteorological stations. These limitations increase the uncertainty of model simulations.

3.1.2 Permafrost temperature and active layer thickness

The temperatures measured at boreholes, which illustrate changes in the thermal state of permafrost, are useful to evaluate ground temperatures simulated by models. Figure 4 shows the locations of boreholes and compares the simulated temperatures at a depth of more than 10 m with borehole observations. Model values were averaged via distance weighting of the four grid cells enclosing each borehole site. The values at the four grid cells corresponded to the observed periods and depths of individual sites. The standard deviation of the offsets in the scatterplot is 3.2ºC, but a comparison of the simulated and observed T_{SOIL} revealed a statistically significant correlation (r = 0.77, P < 0.0001) and a small mean bias of –0.07ºC (Figure 4b), averaged across all sites. In a previous study, CHANGE revealed a cooling bias of –2.1ºC for T_{SOIL} at depths of 0.8–1.2 m (Park et al. 2013a). The improved simulation of T_{SOIL} in this study may be partially attributable to the extension of soil depth to 50.5 m.

Very few long-term and large-scale observations of ALT are available for northern Russia (Frauenfeld et al. 2004), with measurements of T_{SOIL} at only 34 meteorological stations (of which five were newly established during this study). These observations make it possible to compare observed and simulated ALT for the period 1930–1990. Figure 5 presents interannual variability in simulated ALT values in a Russian subregion (60°N–70°N, 115°E–165°E). Simulated ALT values were reasonably correlated with observations for the 61-year period (r = 0.39, P < 0.003). The comparison between observations and simulations shows large differences for the period 1930–1960, compared to similarities during 1960–1990 (r = 0.66, P < 0.0001). Differences are attributable to the low density of stations, together with the scale mismatch between observations and simulations (Dankers et al. 2011; Lawrence et al.

2012; Park et al. 2013a). The model is run at a relatively coarse scale (0.5° latitude/longitude), while observations are essentially at a point scale. Point observations extrapolated to obtain large-area averages tend to be poor representations of true area means. Scale issues generally arise from differences in elevation, climate, soil properties, and landscape, resulting in large heterogeneities in soil thermal and hydraulic properties and hence heterogeneous ALT values. Therefore, the scarcity of stations could further decrease the representation for the averaged ALT of defined eastern Siberia. For example, five or fewer stations were available for the pre-1950 period, when the agreement between observations and simulations was low (Figure 5). The model also suffers from the rough scale in the expression of heterogeneities. The difference in landscape between observations and simulations could also be a reason for their low correlation (Figure 5). Most Russian meteorological stations were generally established over bare land or short grass without thick soil organic layers, while the model considered grid cells surrounding most of the stations within the defined area to be forest with a thick surface organic layer. The dense forest canopy primarily decreases light over the forest floor. The thick organic layer can also effectively reduce heat conductivity, so that the magnitude of the response of T_{SOIL} to climate is smaller in forest than in grassy areas (Park et al. 2013a). More specifically, the inclusion of a peat layer in CHANGE applies to an entire pixel, while peat is not present everywhere in permafrost regions; this can be a key heterogeneity within a pixel and therefore a source of discrepancies in model results relative to single-point observations. Notably, ALT in the observations and simulation was calculated by linear interpolation of the soil temperature between the layer midpoints, which may lead to considerable bias (Dankers et al. 2011).

Simulated ALT values have clearly exhibited an increasing trend during the past 109 years, during which time the average rate of increase was 2.3 cm per decade (r = 0.76, $P <$ 0.0001). Very significant increases in ALT can be seen for the period since 1980, corresponding to increases in air temperature and SND (Figure 6). The model estimated a 4.2-cm increase in ALT for the period 1930–1990, considerably less than the observed increase of 25 cm. Burke et al. (2013) reported increases of 9–16 cm for the same region and period from simulations using the same forcing dataset as that used in this study. Differences in ALT between these two studies are mainly attributable to differences in model structure and scheme, parameters, and initial input data. For

example, CHANGE includes the effects of soil organic carbon on soil thermal and hydrological properties, while Burke et al. (2013) did not consider this variable. This difference is likely an important cause of the different trends in ALT.

3.2 Spatiotemporal variations in snow depth and soil temperature

Figure 6 presents the decadal anomalies for the annual mean SAT, winter SND, and near-surface permafrost temperatures (at depths of 3.6 and 20.4 m) based on the CTRL experiment. The anomalies were relative to means for 1901–2009. The Arctic generally experienced a cold period during the 1960s, and the SAT tended to increase thereafter. In most regions, the strongest warming was apparent during the final decade of the dataset and was particularly significant in Siberia, where positive anomalies exceeded 2ºC in some areas. In the 1940s, the early-twentieth-century warming of the Arctic was discernible in a few areas, but the magnitude of this warming was not as strong as in the final decade of the dataset. SND exhibited large heterogeneous variability. In the 1960s, strong positive SND anomalies were found in coastal regions of Siberia. The same regional variability in SND has also occurred since 1980 when the SAT was warmer. For example, SND in northernmost Siberia displayed strong positive anomalies during 2001–2009. Recent studies have linked the loss of Arctic sea ice to the increased SND in these regions (Ghatak et al. 2011; Cohen et al. 2012; Park et al. 2013b). The open water caused by loss of sea ice is likely to enhance the latent heat flux with the atmosphere and therefore to generate an increase in precipitating clouds over the Arctic (Eastman and Warren 2010; Stroeve et al. 2011). Models have also shown that increased snowfall over Siberia is associated with declining amounts of sea ice (Orsolini et al. 2011).

Soil temperatures at the two depths revealed a general warming trend with substantial spatiotemporal heterogeneities. Soil warming was especially noticeable in the northern tundra. As noted above, air temperature is known to be a major driver of T_{SOIL}. T_{SOIL} increased considerably from 2001 to 2009, consistent with the increase in the SAT. However, the magnitude of soil warming did not relate directly to the degree of SAT warming. For example, the T_{SOIL} in northern Siberia in the 1960s displayed positive anomalies despite SAT cooling. If the SAT dominantly affected T_{SOIL}, soil temperatures would also have cooled, so these findings suggest that snow cover (i.e., increased SND) plays a role. Interestingly, the regions where T_{SOIL} increased closely

572 overlapped with increases in SND. Romanovsky et al. (2010) also reported that
573 increased SND in northwestern Siberia in recent decades has contributed to warmer
574 permafrost temperatures. The decadal variations suggest that the increased SND has
575 combined with warming air temperatures to amplify recent soil warming.
576 Figure 7 presents time series of the regional annual mean (Siberia, 60ºN–70ºN,
577 100ºE–140ºE; North America, 60ºN–70ºN, 120ºW–160ºW) averaged SAT, SND, and
578 $T_{SOIL3.6}$ and $T_{SOIL20.5}$. All variables clearly exhibited increasing trends over the period
579 1901–2009, with statistical significances as high as $P < 0.0001$. The trend in SAT was
580 slightly larger in Siberia than in North America, while the trend in SND was larger in
581 North America, where a post-1990 decrease was observed. T_{SOIL} in North America also
582 simultaneously tended to decrease, probably in response to the lower SND. The trends
583 of T_{SOIL} in North America were only about half as large as those in Siberia. In Siberia,
584 the magnitude of the trend in T_{SOIL} exceeded that of SAT. The larger increases in T_{SOIL}
585 were attributable to the influence of snow cover combined with the SAT. SND
586 explained 49% ($P < 0.0001$) of the soil warming at a depth of 3.6 m compared with
587 20% explained by SAT ($P < 0.0001$). In North America, the corresponding correlation
588 coefficients were 0.56 ($P < 0.0001$) and 0.53 ($P < 0.0001$), respectively, corresponding
589 to 31% and 28% of the variance.
590 In Siberia, the increase in $T_{SOIL3.6}$ was 2.50ºC/century, which is comparable to
591 the 0.26ºC/decade obtained for T_{SOIL} at a depth of 1.6 m, measured at 52 meteorological
592 stations in eastern Siberia (Romanovsky et al. 2007). Observations have revealed a
593 1ºC–2ºC increase in the permafrost temperatures of northern Russia during the last
594 30–35 years (Oberman 2008; Romanovsky et al. 2010; Drozdov et al. 2012). The
595 permafrost in North America has also warmed by 0.5ºC–2ºC during the past three
596 decades (Osterkamp 2008; Smith et al. 2010). The increase in permafrost temperatures
597 is undeniable, although the rate of increase varies regionally. Notably, the rates of
598 increase during recent decades have been exceptionally strong compared with the
599 century-scale simulated trend.
600
601 3.3 Model experiments
602 3.3.1 Near-surface permafrost sensitivity to snow depth
603 Figure 8 presents historical simulations of the extent of near-surface
604 permafrost from individual experiments (see Table 1 for an explanation of the

605 abbreviations). Here, "permafrost" is defined as the ground of each grid cell being
606 frozen for 2 or more consecutive years in at least one soil layer within the depth of the
607 lowest boundary. The analysis considered two cases of the bottom boundary (3.6 and
608 50.5 m). The extent of permafrost represents an integrated permafrost area in the
609 pan-Arctic region poleward of 45ºN. Noticeable and consistent degradation of the
610 extent of permafrost occurred over the 109 years. Here, degradation of permafrost refers
611 to an expansion of the area where ALT exceeds the bottom boundary, rather than
612 permafrost being completely absent. This degradation was relatively small before 1940
613 and increased after 1980 when the SAT evidently entered into the warming phase
614 (Figure 6a). However, the two cases of the bottom boundary resulted in large
615 differences in the magnitude of permafrost degradation. The disappearance of
616 permafrost from the upper 3.6 m occurred over areas from 1.46 to 3.36 million km^2 in
617 all experiments over the 109 years, approximately 2–2.5 times larger than
618 corresponding degradations (0.81–1.47 million km^2) in the case of 50.5 m. Previous
619 simulations also projected the degradation of the near-surface permafrost to range from
620 1 to 4 million km^2 during the last century (Lawrence et al. 2008; Burke et al. 2013). In
621 many permafrost environments, the base immediately below the maximum ALT tends to
622 be ice-rich (Shur et al. 2005). CHANGE did not include excess ice, but tended to
623 simulate saturated moisture content (ice plus liquid water) at the base layer of the ALT.
624 The presence of the ice layer critically controls the potential increase in ALT, owing to
625 latent heat effects, consequently retarding the rate of permafrost degradation. Figure 8
626 emphasizes the importance of the bottom soil boundary extension when assessing
627 historical and future variations, and trends of permafrost in the Northern Hemisphere.
628 Despite the broad similarities in the variability of permafrost extent simulated
629 in the different experiments, several important differences appeared. More winter
630 precipitation produces deeper SND, further insulating the soil and thus resulting in a
631 reduction in the extent of permafrost. In contrast, a decrease in SND enhances soil
632 cooling, leading to less permafrost being lost. However, the absolute magnitude of the
633 change in the extent of permafrost was larger when SND increased than when it
634 decreased. Increased SND resulted in higher total permafrost loss than in experiments in
635 which SND decreased (Table 2). Differences in the timing of changes in snow cover
636 also led to large differences in permafrost extent. Changes in snow cover during early
637 winter (October–December) affected permafrost warming/cooling more significantly

than changes during midwinter (December–February). An increase in SND from October to December resulted in a permafrost loss of about 0.4 million km^2 more than an increase during December–February (Table 2). Zhang (2005) suggested that increased snowfall during October and November effectively increases T_{SOIL} through earlier insulation. Moreover, increased SND results in extremely large temperature gradients between the snow and soil surface, which can generate a depth hoar layer that persists until snowmelt and acts as a strong insulator (Zhang et al. 1996).

Many studies have concluded that over the last few decades, changes in the SAT alone cannot account for changes in T_{SOIL}, which are the result of a complex response to the combination of snow cover and air temperature (Zhang 2005). However, they are well explained by the results of both DN_T_H and UP_T_L (Figure 8). The permafrost extent in DN_T_H was similar to that in the CTRL during the period 1901–1940, owing to the influence of a higher SAT held at 1991–2009 climatological levels, which readily offset soil cooling caused by a decreased SND. Thereafter, however, the influence of SAT in DN_T_H on T_{SOIL} was relatively diminished due to the decrease in the SAT scaling rate. Likewise, the degradation rate of permafrost in DN_T_H also decreased, and the permafrost extent reached a state similar state to DN_{O_F} during the 2000s (Figure 8a). This is attributable to enhanced soil cooling induced by a shallower SND relative to thermal influences of SAT. Alternatively, the deeper SND in UP_T_L strongly insulated the soil, resulting in higher permafrost degradation until the early 1970s when the SAT was colder, equivalent to the degradations in experiments with increased SND. Thereafter, the degradation rate of permafrost weakened (Figure 8a). Increased SND readily contributes to soil warming. Conversely, snow-related high albedo and latent heat for fusion could retard soil thawing during spring. Moreover, reduced thermal forcing induced by a lower SAT scaling rate could be related to late snowmelt, as well as reduced soil thawing during summer. However, when the lowest boundary was extended to 50.5 m, permafrost extents of both DN_T_H and UP_T_L during the 2000s ranked higher among the same types of snow experiments (Figure 8b). The extension of the lowest boundary increased the thermal damping depth, thereby enhancing a time lag and diminishing the surface thermal signal. Together, snow cover limits the penetration of cold, although magnitudes of insulation differ, depending on snow thickness. Stieglitz et al. (2003) reported that borehole temperatures at a depth of 20 m, observed at Barrow, tracked the variability of snow cover independently of the

671 SAT.
672
673 3.3.2 Snow depth
674 The average winter (DJF) SND in individual experiments from 1981 to 2009
675 was expressed as a difference relative to the CTRL (Figure 9). Precipitation treatments
676 in the cold season were expressed as changes in SND: increased precipitation resulted in
677 greater SND and vice versa. SND changed significantly in regions poleward of 55ºN.
678 The greatest changes appeared in northern Siberia and northeastern Canada
679 (approximately 15 cm or more), with a maximum regional change of approximately 30
680 cm. These regions originally maintained a deeper SND during winter, ranging from 50
681 to 90 cm. This greater depth resulted in relatively large rates of change in SND in terms
682 of changing precipitation. For example, data from ROSHYDROMET meteorological
683 stations revealed that the maximum winter SND in northwestern Siberia ranged from 40
684 to 150 cm (Romanovsky et al. 2010), in which the linear trend of the SND corresponded
685 to increases of 6–8 cm/decade during 1966–2007 (Bulygina et al. 2009).
686
687 3.3.3 Active layer and freezing thickness
688 The simulated T_{SOIL} at grid pixels that were defined as permafrost were
689 linearly interpolated to determine the depth at which T_{SOIL} crossed the 0ºC isotherm.
690 The maximum depth over an annual cycle was defined as the ALT of that year. Figure
691 10 presents differences in ALT between the model experiments and CTRL. ALT is
692 known to primarily depend on the cumulative thermal history of the ground surface
693 during the summer thaw (Osterkamp 2007). However, we found that snow cover also
694 affected the variability of ALT. Deeper snow contributed to a larger ALT, and shallower
695 snow resulted in a smaller ALT (Figure 10a and b). The sensitivity of the ALT to
696 changes in snow cover was significant in the southern boundary regions of the
697 permafrost area, where the maximum difference in ALT was ±20 cm. In southern
698 forested zones, the combined impacts of surface vegetation and snow cover contributed
699 to soil thermal warming during winter. Vegetation increases the air temperature thawing
700 index (e.g., accumulated thawing degree days), which is required for soil thawing
701 (Nixon and Taylor 1998). Southern zones also have larger thawing indices and longer
702 thawing seasons. The relatively warm permafrost in southern forested zones forms
703 nearly vertical T_{SOIL} profiles with small temperature gradients. Responding to the

704 outside forcing, the small temperature gradient facilitates changes in the depth of the
705 0ºC isotherm. In addition to producing a higher temperature, snow cover favors a deeper
706 ALT, so the response of ALT to snow cover is more sensitive in southern forested zones
707 than in northern regions.

708 The response of the ALT to SND was complicated by the influence of other
709 processes and their interactions. For example, under conditions of deeper SND and a
710 cold SAT (UP_T_L; Figure 10c), the SND insulated the soil during winter, but if the SND
711 remained thick in late spring or early summer, it had a reverse cooling effect because of
712 its albedo and the use of latent heat of fusion. The cold SAT also weakened the soil
713 thawing process, which was discernible over wide areas. In contrast, the combination of
714 a reduced SND and a warm SAT resulted in a positive and negative ALT in the northern
715 and southern regions, respectively (DN_T_H; Figure 10d). The reduction in SND could
716 lead to more soil freezing in the northern regions. However, the warm SAT reduced the
717 freezing index and could lead to an earlier snowmelt. Under these conditions, the warm
718 SAT during summer could contribute to a deeper ALT. The SND in the southern regions
719 then became thinner, and the ALT deepened. Therefore, the soil freezing induced by the
720 thinner SND required more heat for the ALT to reach its original depth. The reduced
721 SND also made a relatively low contribution to soil moisture. The southern region is
722 covered with vegetation that consumes large amounts of soil water during the summer
723 season. The resulting dry soil had a relatively low thermal conductivity, and therefore a
724 thinner ALT.

725 Seasonal maximum freezing thickness (FRT) was calculated for grid cells that
726 were classified as non-permafrost. Figure 11 displays the differences in FRT between
727 each experiment and the CTRL for the period 1981–2009. FRT was sensitive to the
728 variability of SND, especially near the permafrost boundary, where the maximum
729 difference of FRT was ±40 cm. A thicker SND reduced the FRT (Figure 11a), which
730 was discernible under the cold SAT, except for some regions where the SND was
731 originally thin (Figure 11c). In contrast, a decrease in the SND resulted in a deepened
732 FRT (Figure 11b), even when the SAT was warmer (Figure 11d). While the Arctic
733 winter SAT has increased during recent decades (Bekryaev et al. 2010), the winter is
734 still sufficiently cold for the ground to freeze. Thus, the magnitude of soil freezing was
735 strongly dependent on the change in snow cover, especially in colder regions within the
736 zone of seasonal freezing.

737

738 3.3.4 Soil temperature

739 The influences of changed seasonal snow on T_{SOIL} at depths of 3.6 and 20.4 m
740 were averaged for the period 1981–2009. Figure 12 presents the differences in the
741 average T_{SOIL} between each experiment and the CTRL. Increased SND clearly increased
742 the T_{SOIL}, while decreased SND decreased it (Figure 12a and 12b). Although large
743 spatial heterogeneities appeared in the differences, the differences were generally larger
744 in northern regions than in the south. This pattern differs from that of the ALT, which
745 was more sensitive to changes in snow cover in the south (Figure 10). Northern regions
746 are characterized by a longer freezing season (8–9 months). Considerable energy is
747 required to thaw the frozen soil in this cold northern permafrost. Moreover, the ice- and
748 peat-rich permafrost further limits soil thawing. Therefore, the ground thermal regime
749 of these regions is strongly dependent on the magnitude of the thermal offset created by
750 snow cover. In northeastern Siberia, the increased $T_{SOIL3.6}$ during the 109-year study
751 period exceeded that of the SAT due to the insulating effect of snow cover (Figure 7).
752 Zhang et al. (1997) observed that in northern Alaska, seasonal snow cover induced
753 increases of 3ºC–7ºC in the mean annual permafrost surface temperatures.

754 The absolute values of the differences in T_{SOIL} generally tended to be larger
755 when the SND decreased than when it increased. A change in an area with deeper SND
756 in the winter could have a smaller effect than the same changes in an area with
757 shallower SND because snow insulation varies more strongly at shallow depths (Park et
758 al. 2014). This is evident in Figure 13, which shows the average differences between
759 each experiment and the CTRL for northeastern Siberia and western North America
760 (defined in Figure 7). In northeastern Siberia, for example, the average differences in
761 $T_{SOIL20.4}$ for UP_{O_F} and DN_{O_F} were 0.75ºC and –1.4ºC, respectively. Differences in
762 western North America were less than 50% of those in northeastern Siberia (Figure 13b).
763 Zhang (2005) explained that the insulation effect of snow cover becomes less
764 pronounced when the winter SND exceeds 40–50 cm. In the model results, this
765 threshold effect can be seen in northwestern Siberia and northeastern Canada, where the
766 SND was quite thick (Figure 9). This original SND (Figure 9) remained relatively thick
767 even when winter precipitation was increased or decreased in the experiments.
768 Therefore, the differences in T_{SOIL} were very small (Figure 12). In the combined case of
769 a lower SND and a warm SAT (DN_T_H), the warm SAT clearly affected T_{SOIL}. The

770 contribution is represented by the differences between DN_{O_F} and DN_T_H, (Figure 13).
771 The difference in $T_{SOIL20.4}$ in northeastern Siberia was 0.24ºC. However, the lower SND
772 offset the warming impact of the SAT, which resulted in soil cooling (Figure 12d). This
773 cooling was observed over a wide area, but not in some southern regions where the
774 SND was thin and the SAT was relatively warm. The combination of a thicker SND and
775 a cold SAT (UP_T_L) resulted in an increase of T_{SOIL} in permafrost-covered regions and a
776 cooling in the remaining regions (Figure 12c), in contrast to DN_T_H (Figure 12d). These
777 experiments indicate that T_{SOIL} in the northern permafrost region was more sensitive to
778 changes in SND than those in SAT.
779 The differences in $T_{SOIL20.4}$ for individual experiments (Figure 12) were
780 zonally averaged for individual latitudes. The meridional profiles formed a cylindrical
781 tree shape and reached a maximum at approximately 70ºN (Figure 14). The results at
782 3.6 m were similar, although the values differed. Among the important results shown in
783 Figure 14, T_{SOIL} tended to be more sensitive to changes in SND in northern regions,
784 particularly in the 60ºN–80ºN zone. T_{SOIL} was also most sensitive to changes in SND
785 during the early winter season, in situations when SND either increased or decreased
786 (Figure 13). For example, the cooling in DN_{O_D} was 0.3ºC–0.5ºC greater than in DN_{D_F}
787 in the 60ºN–80º°N zone. Where the SND increased, the relatively small differences in
788 T_{SOIL} between the experiments illustrate the nonlinear relationship between changes in
789 snow cover and the insulation effect.
790 A shallower SND enhances the thermal cooling of soil during winter. Cooling
791 during winter results in a high annual thermal amplitude. In contrast, in these
792 experiments, the warming of T_{SOIL} resulting from a thicker SND reduced the annual
793 amplitude of T_{SOIL}. This behavior is apparent in Figure 15, which shows the seasonal
794 variations of SND and T_{SOIL} at the soil surface and at a depth of 3.6 m in northeastern
795 Siberia (60ºN–70ºN, 100ºE–140ºE) averaged during the period 1981–2009. In all
796 experiments, the seasonal cycle of SND peaked in February, when the maximum
797 difference between DN_T_H and UP_T_L was 23 cm. At the soil surface, the model
798 simulations had annual amplitudes ranging from 20ºC to 25ºC. The difference in the
799 amplitude between UP_{O_F} and DN_{O_F} was approximately 5ºC, which reflects the
800 difference in the insulation caused by their SND differences of more than 20 cm during
801 winter. At the soil surface, a thicker SND also leads to a relatively low thermal
802 amplitude at a depth of 3.6 m (Figure 15, right panel). For example, the annual

amplitude in UP_{O_F} is 3.0ºC, the minimum among all experiments. In contrast, the maximum amplitude (approximately 6.3ºC) was found in DN_{O_F}. These two experiments produced the largest T_{SOIL} difference (3.2ºC) in April, which represents the magnitude of the SND-induced difference. This difference persisted over summer and clearly affected the difference in the annual mean T_{SOIL}.

3.4 Contributions of SAT and SND to T_{SOIL}

To examine the relative contributions of SND and the SAT to changes in T_{SOIL}, we used multilinear regressions to calculate the proportion of T_{SOIL} variance that could be explained by SND and the SAT. The multilinear regression method is useful when explanatory variables are linearly independent. However, the SAT and SND are partly correlated. Therefore, the fraction of the variation in T_{SOIL} that the SAT and SND explain individually includes a correlation that overlaps the explanatory variables. The correlation was removed by calculating a regression of the SAT and SND (Legendre and Legendre 1998). The CTRL simulation results for 1971–2009 were used for this analysis. Figure 16 shows the fractions of the variance in $T_{SOIL3.6}$ that could be individually explained by the annual mean SAT and winter SND. The results demonstrate that SND contributed more than the SAT to $T_{SOIL3.6}$ in northeastern Siberia, an area underlain by permafrost, wherein SND explained 50% or more of the total variation in $T_{SOIL3.6}$. This percentage was greater than or equal to the contribution of the SAT. Our assessment is generally consistent with previous studies (Stieglitz et al. 2003; Osterkamp 2007; Lawrence and Slater 2010; Park et al. 2014). Where the influence of SND was lowest, the impact of the SAT dominated.

4. Discussion and Conclusion

This study examined the influence of snow cover on T_{SOIL} under the climatic conditions of the twentieth and early twenty-first centuries, based on model experiments that considered winter precipitation and air temperature. The results demonstrated that snow cover has a substantial impact on T_{SOIL} in northernmost regions, particularly those with continuous permafrost (Figure 12). They suggest that in addition to SAT warming, snow may further enhance permafrost-related feedbacks. The large and historically inert soil carbon pool (Tarnocai et al. 2009) could be exposed to decomposition as the permafrost thaws, thereby amplifying both Arctic and global climate change. A

sensitivity study using a land surface model found that higher T_{SOIL} caused by snow insulation yielded an increase of 22% in the respiration rate over the pan-Arctic region, and resulted in both a reduction in the extent of permafrost and a deeper ALT that exposed greater volumes of soil to microbial decomposition (Gouttevin et al. 2012). The thawing of permafrost could also play an important role under local hydrological conditions. Northeastern Siberia is characterized by ice-rich permafrost called Yedoma (Strauss et al. 2013). Thawing of this ice-rich permafrost in response to ground warming could produce excessive soil water. The Gravity Recovery and Climate Experiment conducted satellite observations and identified an increase in terrestrial water storage over eastern Siberia during the past decade, suggesting the melting of excess ground ice (Landerer et al. 2010). The resulting increase in surface water also contributed to the extension of wetland areas (Fedorov et al. 2014), which strongly controls the seasonal evolution of carbon and methane.

Six models using the IPCC A2 emissions scenario predicted that the maximum monthly snow water equivalent for the period 2049–2060 will increase by 0%–15%, compared with the period 1970–1999 over much of the Arctic, with larger increases (15%–30%) over the Siberian sector. However, the autumn-to-spring snow season length was shortened. Increased air temperature also causes midwinter snowmelt and compaction (Callaghan et al. 2011). These climate change-associated changes could alter the structure and properties of snow cover, affecting the soil thermal regime. In reality, we have already seen several changes in the physical properties of the Arctic snow cover over the last few decades, particularly the development of more snow and ice layers in the snowpack (Bulygina et al. 2010; Shmakin 2010; Johansson et al. 2011; Liston and Hiemstra 2011). In the Arctic, however, snow tends to have ecosystem-specific properties (Sturm et al. 1995), which are generally associated with particular landscapes and climates, especially local wind conditions. On the tundra, snow consists of hard, low-density, wind-packed surface layers with coarse and low-density depth hoar layers at the base (Benson and Sturm 1993). Increases in fresh snow are likely to increase the depth hoar fraction within the snowpack, reducing thermal conductivity and consequently increasing T_{SOIL}. Model sensitivity analysis has revealed that thermal conductivity decreases nonlinearly with increasing depth of the hoar fraction (Zhang et al. 1996). Along the Alaskan Arctic coast, changes in the depth of the hoar fraction (from 0 to 0.6) resulted in a decrease in the annual amplitude of the

ground surface temperature by 6.3ºC (Zhang et al. 1996). In boreal forest, snow is characterized by deeper depth hoar layers and no wind slab (Sturm et al. 1995). Vegetation has a sheltering function that traps and redistributes snow, which could lead to a greater depth of the hoar fraction and an increased SND (Sturm and Johnson 1992). However, a vegetation canopy also shades the soil surface, resulting in cooling during summer. This shading effect may compete with the insulating effect of winter snow cover on the ground thermal regime. However, in northern regions with relatively long freezing periods, both increased SND and changes in the snow structure are favorable to soil thermal warming. Taken together with future projections, the results of this study suggest that snow cover could result in warmer ground temperatures in northern regions, particularly in areas covered by continuous permafrost.

A novel finding of this study is that an extension of the bottom soil boundary results in a greater extent of permafrost. In the early twenty-first century, for example, the extent of permafrost in the 50.5-m lower boundary was 1.2–2.9 million km^2 greater than that in a 3.6-m lower boundary (Figure 8 and Table 2), suggesting that the expansion of permafrost has an ALT deeper than 3.6 m. Using model experiments, we found that permafrost degradation mainly occurred at southern boundary regions. The same phenomenon was also identified in southern Canada (Zhang et al. 2006). The increase in ALT is attributable to an increase in T_{SOIL}. In the CTRL experiment, T_{SOIL} at the permafrost southern boundary increased by approximately 0°C–2°C during 2001–2009, except in some areas (Figure 6c). An increased T_{SOIL} is enough to drive a deepening of ALT. Smith et al. (2010) observed that T_{SOIL} at a depth of 4 m at sites in northern Quebec had, on average, increased by 1.9°C during 1993–2008, which contributed to the increase in ALT, ranging from 3 to 992 cm. ALTs of >3.6 m have indeed been observed at several sites of discontinuous permafrost, such as in Mongolia (CALM, http://www.gwu.edu/~calm/) and Canada (Smith et al. 2010). However, a number of models defined a shallower bottom soil boundary. For example, most Coupled Model Intercomparison Project Phase 5 (CMIP5) models limited the lower boundary to a depth of <15 m, simulating a permafrost area of 1.4–17.4 million km^2 in 2005 (Koven et al, 2013) compared to our CTRL result of 19.3 million km^2 (Table 2). The deepening of soil increases the thermal damping depth and alleviates the surface thermal signal, consequently limiting the speed of permafrost degradation. Alexeev et al. (2007) suggested that a soil depth of at least 30 m is needed to simulate annual and

902 decadal cycles of temperature dynamics for permafrost. Future climate warming may
903 enhance ALT (Koven et al. 2013). Under such conditions, however, a shallower soil
904 boundary could underestimate the permafrost area, which can inductively increase
905 uncertainties of permafrost-associated interactions and feedbacks; we thus suggest that a
906 new configuration of the model soil layer is needed for permafrost simulations.
907 The current atmospheric warming has led to the warming and degradation of
908 permafrost, with potential feedback consequences for biogeochemical and hydrological
909 cycling in the Arctic, and therefore for the global climate. In this attempt to clarify the
910 ongoing changes in permafrost, especially the relative importance of drivers, we used
911 the CHANGE model to simulate permafrost variability over multi-decadal time periods
912 and at the pan-Arctic spatial scale. An important finding is the significant impact of
913 snow cover on changes in the permafrost over the northernmost regions. We have
914 quantified this effect.
915 Snowfall largely depends on atmospheric circulation patterns. This
916 dependence introduces uncertainty into the magnitude of future changes in snowfall,
917 which could in turn increase uncertainty in the expression of climate warming, its
918 effects on soil thermal status, and the distribution of permafrost. Ecosystem-dependent
919 snow physical properties remain poorly represented in terrestrial models. Improved
920 representation of these properties, including the development of subgrid-scale snow
921 modules, is a priority for future work.
922
923 Acknowledgments. This work was supported in part by the JAMSTEC-IARC
924 Collaboration Study (JICS) and Research Project No. C-07 of the Research Institute for
925 Humanity and Nature (RIHN). We thank Dr. K. Oshima for useful discussions and
926 comments, Dr. R. Brown (Environmental Canada) for the provision of snow data, and
927 anonymous reviewers for critical comments and suggestions for our paper.
928
929
930 References
931 Adam JC, Lettenmaier DP (2003) Adjustment of global gridded precipitation for
932 systematic bias. J Geophys Res 108, D9. doi: 10.1029/2002JD002499
933 Alexeev VA, Nicolsky DJ, Romanovsky VE, Lawrence DM (2007) An evaluation of
934 deep soil configurations in the CLM3 for improved representation of permafrost.

935 Geophys Res Lett 34:L09502. doi:10.1029/2007GL029536
936 Bekryaev RV, Polyakov IV, Alexeev VA (2010) Role of polar amplification in long-term
937 surface air temperature variations and modern Arctic warming. J Clim 23:3888–3906.
938 doi:10.1175/2010JCLI3297.1
939 Benson CS, Sturm M (1993) Structure and wind transport of seasonal snow on the
940 Arctic slope of Alaska. Ann Glaciol 18:261–267
941 Boike J, Kattenstroth B, Abramova K (2013) Baseline characteristics of climate,
942 permafrost and land cover from a new permafrost observatory in the Lena River Delta,
943 Siberia (1998–2011). Biogeosciences 10:2105–2128. doi:10.5194/bg-10-2105-2013
944 Brown RD (2000) Northern Hemisphere snow cover variability and change, 1915–1997.
945 J Clim 13:2339–2355
946 Bulygina ON, Razuvaev V, Korshunova N (2009) Change in snow cover northern
947 Eurasia in the last decades. Environ Res Lett 4, 045026.
948 doi:10.1088/17489326/14/4/045026
949 Bulygina ON, Groisman PY, Razuvaev VN Radionov VF (2010) Snow cover basal ice
950 layer changes over Northern Eurasia since 1966. Environ Res Lett 5, 015004.
951 doi:10.1088/1748-9326/5/1/015004
952 Burke EJ, Kankers R, Jones CD, Wiltshire AJ (2013) A retrospective analysis of pan
953 Arctic permafrost using the JULES land surface model. Clim Dyn
954 doi:10.1007/s00382-012-1648-x
955 Burn CR, Kokelj SV (2009) The environment and permafrost of the Mackenzie Delta
956 area. Permaf Periglac Process 20(2):83–105
957 Callaghan T, Johansson M, Brown R, Groisman P, Labba N, Radionov V (2011)
958 Changing snow cover and its impacts, in AMAP, 2011, Snow, Water, Ice and Permafrost
959 in the Arctic (SWIPA): Climate Change and the Cryosphere, Arctic Monitoring and
960 Assessment Programme (AMAP), Oslo, Norway, pp 538
961 Cohen J, Furtado J, Barlow M, Alexeev V, Cherry J (2012) Arctic warming, increasing
962 snow cover and widespread boreal winter cooling. Environ Res Lett 7, 014007.
963 doi:10.1088/1748-9326/1/1/014007
964 Dankers R, Burke EJ, Price J (2011) Simulation of permafrost and seasonal thaw depth
965 in the JULES land surface scheme. Cryosphere 5:773–790. doi:10.5194/tc-5-773-2011.
966 Drozdov DS, Ukraintseva NG, Tharev AM, Chekrygina SM (2010) Permafrost
967 temperature fields changes and Urengoi gas-field geosystems condition in the last

968 35-year (1974–2008). Earth Cryosphere 14(1):22–31 (in Russian)
969 Drozdov DS, Malkova GV, Ukraintseva NG, Korostelev YV (2012) Permafrost
970 monitoring of southern Tundra landscapes in the Russian European North and West
971 Siberia. TICOP, Vol. 2, 65–69
972 Eastman R, Warren SG (2010) Interannual variations of Arctic cloud types in relation to
973 sea ice. J Clim 23:4216–32
974 Fedorov AN, Gavriliev PP, Konstanitinov PY, Hiyama T, Iijima Y, Iwahana G (2014)
975 Estimating the water balance of a thermokarst lake in the middle of the Lena River
976 basin, eastern Siberia. Ecohydrology 7:188–196. doi:10.1002/eco.1378
977 Frauenfeld OW, Zhang T, Barry RG, Gilichinsky D (2004) Interdecadal changes in
978 seasonal freeze and thaw depths in Russia. J Geophys Res 109, D05101.
979 doi:10.1029/2003JD004245
980 Ghatak D, Gong G, Frei A (2010) North American temperature, snowfall, and
981 snow-depth response to winter climate modes. J Clim 23:2320–2332.
982 doi:10.1175/2009JCLI3050.1
983 Gouttevin I, Menegoz M, Domine F, Krinner G, Koven C, Ciais P, Tarnocai C, Boike J
984 (2012) How the insulating properties of snow affect soil carbon distribution in the
985 continental pan-Arctic area. J. Geophys Res 117, G02020. doi:10.1029/2011JG001916
986 Hinzman LD, Coauthors (2005) Evidence and implications of recent climate change in
987 Northern Alaska and other Arctic regions. Clim Change 72:251–298.
988 doi:10.1007/s10584-005-5352-2.
989 IPCC (2014) Climate Change 2013: The Physical Science Basis. Fifth Assessment
990 Report of the Intergovernmental Panel on Climate Change, Cambridge University Press,
991 Cambridge, UK, in press.
992 Johansson G, Pohjola VA, Jonasson C, Callaghan TV (2011) Multi-decadal changes in
993 snow characteristics in sub-Arctic Sweden. Ambio 40:566–574
994 Jones PD, New M, Parker PE, Martin S, Rigor IG (1999) Surface air temperature and its
995 changes over the past 150 years. Rev Geophys 37:173–199
996 Konstantinov PV (2009) Manual on monitoring site establishment for permafrost
997 temperature observation. Melnikov Permafrost Institute Press, Yakutsk, pp 68 (in
998 Russian)
999 Koven CD, Ringeval B, Friedlingstein P, Ciais P, Cadule P, Khvorostyanov D, Krinner
1000 G, Tarnocai C (2011) Permafrost carbon-climate feedbacks accelerate global warming.

1001 PNAS 108:14769–14774. doi:10.1073/pnas.1103910108
1002 Koven CD, Riley WJ, Stern A (2013) Analysis of permafrost thermal dynamics and
1003 response to climate change in the CMIP5 earth system models. J Clim 26:1877–1900.
1004 doi:10.1175/JCLI-D-12-00228.1
1005 Lachenbruch AH, Marshall BV (1986) Changing climate: Geothermal evidence from
1006 permafrost in the Alaskan Arctic. Science 234:689–696
1007 Landerer FW, Dickey JO, Güntner A (2010) Terrestrial water budget of the Eurasian
1008 pan-Arctic from GRACE satellite measurements during 2003–2009. J Geophys Res 115,
1009 D23115. doi:10.1029/2010JD014584
1010 Lawrence DM, Slater AG (2008) Incorporating organic soil into a global climate model.
1011 Clim Dyn 30:145–160, doi:10.1007/s00382-007-0278-1
1012 Lawrence DM, Slater AG (2010) The contribution of snow condition trends to future
1013 ground climate. Clim Dyn 34, doi:10.1007/s00382-009-0537-4
1014 Lawrence DM, Slatter AG, Swenson SC (2012) Simulation of present-day and future
1015 permafrost and seasonally frozen ground conditions in CCSM4. J Clim 25:2207–2225.
1016 doi:10.1175/JCLI-D-11-00334.1
1017 Legendre P, Legendre LFJ (1998) Numerical ecology. Elsevier, Amsterdam, The
1018 Netherlands, pp 853
1019 Liston GE, Hiemstra CA (2011) The changing cryosphere: Pan-Arctic snow trends
1020 (1979–2009). J Clim 24:5691–5712. doi:10.1175/JCLI-D-11-00081.1
1021 Malkova GV (2008) The last twenty-five years of changes in permafrost temperature of
1022 the European Russian Arctic. In: Proceedings of the Ninth International Conference on
1023 Permafrost. Edited by Kane DL and Hinkel KM. Fairbanks. Institute of Northern
1024 Engineering, University of Alaska Fairbanks, June 29–July 3, Fairbanks, Alaska, Vol. 2,
1025 1119–1124
1026 Meehl GA, Stocker TF, Collins W, Friedlingstein P, Gaye A, Gregory J, Kitoh A, Knutti
1027 R, Murphy J, Noda A, Raper S, Watterson I, Weaver A, Zhao ZC (2007) Global climate
1028 projections. In: Solomon S. et al. (eds) Climate change 2007: the physical science basis.
1029 Cambridge University Press, London, pp. 747–845
1030 Moskalenko NG (2009) Ground temperature changes and vegetation under climate
1031 changing and anthropogenic influence in Nadym region of West Siberia. Earth
1032 Cryosphere 13(4):18–23 (in Russian)
1033 Murzin YA, Rusakov VG (1996) Ground temperature in the Yana basin, Cryolithozone

1034 and underground water in Siberia. Vol.1. Cryolithozone morphology-Yakutsk, MPI
1035 press, pp. 45–56 (in Russian)
1036 Nelson FE (2004) Circumpolar active layer monitoring (CALM) Workshop. Permaf
1037 Periglac Process 15(2):99–188
1038 Nixon FM, Taylor AE (1998) Regional active layer monitoring across the sporadic,
1039 discontinuous and continuous permafrost zones, Mackenzie Valley, Northwestern
1040 Canada. In: Proceedings of the 7th International Conference on Permafrost, June 23–27,
1041 1998, Yellowknife, Canada, Nordicana, Lewkowicz AG, Allard M (eds), vol. 57, pp
1042 815–820
1043 Oberman NG (2007) Global warming and cryolithozone changes in Pechora-Urals
1044 regions. Razvedka I ohrana nedr 4:63–68 (in Rissian)
1045 Oberman NG (2008) Contemporary permafrost degradation of the European north of
1046 Russia. In: Proceedings of the Ninth International Conference on Permafrost. Edited by
1047 Kane DL and Hinkel KM. Fairbanks. Institute of Northern Engineering, University of
1048 Alaska Fairbanks, June 29–July 3, Fairbanks, Alaska, Vol. 2, pp. 1305–1310
1049 Oelke C, Zhang T, Serreze M (2004) Modeling evidence for recent warming of the
1050 Arctic soil thermal regime. Geophys Res Lett 31:L07208. doi:10.1029/2003GL019300
1051 Orsolini YJ, Senan R, Benestad RE, Melsom A (2011) Autumn atmospheric response to
1052 the 2007 low Arctic sea ice extent in coupled ocean–atmosphere hindcasts. Clim Dyn
1053 114, D19108
1054 Osterkamp TE (2007) Characteristics of the recent warming of permafrost in Alaska. J
1055 Geophys Res 112, F02S02. doi:10.1029/2006JF000578
1056 Osterkamp TE (2008) Thermal state of permafrost in Alaska during the fourth quarter of
1057 the twentieth century. In: Proceedings of the Ninth International Conference on
1058 Permafrost. Edited by Kane DL and Hinkel KM. Fairbanks. Institute of Northern
1059 Engineering, University of Alaska Fairbanks, June 29–July 3, Fairbanks, Alaska, Vol. 2,
1060 pp. 1333–1338
1061 Park H, Iijima Y, Yabuki H, Ohta T, Walsh J, Kodama K, Ohata T (2011a) The
1062 application of a coupled hydrological and biogeochemical model (CHANGE) for
1063 modeling of energy, water, and CO_2 exchange over a larch forest in eastern Siberia. J
1064 Geophys Res 116, D15102. doi:10.1029/2010JD015386
1065 Park H, Yabuki Y, Ohata T (2011b) Analysis of satellite and model datasets for
1066 variability and trends in Arctic snow extent and depth, 1948–2006. Polar Sci

1067 doi:10.1016/j.polar.2011.11.002
1068 Park H, Walsh J, Fedorov AN, Sherstiukov AB, Iijima Y, Ohata T (2013a) The influence
1069 of climate and hydrological variables on opposite anomaly in active-layer thickness
1070 between Eurasian and North American watersheds. Cryosphere 7:631–645.
1071 doi:10.5194/tc-7-631-2013
1072 Park H, Walsh JE, Kim Y, Nakai T, Ohata T (2013b) The role of declining Arctic sea ice
1073 in recent decreasing terrestrial Arctic snow depths. Polar Sci 7:174–187.
1074 doi:10.1016/j.polar.2012.10.002
1075 Park H, Sherstiukov AB, Fedorov AN, Polyakov IV, Walsh JE (2014) An
1076 observation-based assessment of the influences of air temperature and snow depth on
1077 soil temperature in Russia. Environ Res Lett 9:064026.
1078 doi:10.1088/1748-9326/9/6/064026
1079 Pavlov AV, Moskalenko NG (2001) Soils thermal regime in the. Earth Cryosphere
1080 5(2):11–19 (in Russian)
1081 Peterson B, Coauthors (2002) Increasing river discharge to the Arctic Ocean. Science
1082 298:2171–2173
1083 Romanovsky VE, Sazonova TS, Balobaev VT, Shender NI, Sergueev DO (2007) Past
1084 and recent changes in air and permafrost temperatures in eastern Siberia. Global
1085 Planetary Change 56:399-413
1086 Romanovsky VE, Drozdov DS, Oberman NG, Malkova GV, Kholodov AL, Marchenko
1087 SS, Moskalenko NG, Sergeev DO, Ukraintseva NG, Abramov AA, Gilichinsky DA,
1088 Vasiliev AA (2010) Thermal state of permafrost in Russia. Permaf Periglac Process
1089 21:136–155. doi:10.1002/ppp.683
1090 Schindler DW, Donahue WF (2006) An impending water crisis in Canada's western
1091 prairie provinces. PNAS 103:7210-7216. doi:10.1073/pnas.0601568103
1092 Schuur EA, Vogel JG, Crummer KG, Lee H, Sickman JO, Osterkamp TE (2009) The
1093 effect of permafrost thaw on old carbon release and net carbon exchange from tundra.
1094 Nature 459:556–559. doi:10.1038/nature08031
1095 Sergueev DO, Ukhova JA, Stanilovskaya JV, Romanovsky VE (2007) Temperature
1096 regime of the permafrost and the active layer in northern Transbaykalia mountains
1097 (recommencement of Fixedwsite observations). Earth Cryosphere 11(2):19–26 (in
1098 Russian)
1099 Shiklomanov NI, Streletskiy DA, Nelson FE, Hollister RD, Romanovsky VE, Tweedie

1100 CE, Bockheim JG, Brown J (2010) Decadal variations of active-layer thickness in
1101 moisture-controlled landscapes, Barrow, Alaska. J Geophys Res 115:G00104.
1102 doi:10.1029/2009JG001248
1103 Shur Y, Hinkel KM, Nelson FE (2005) The transient layer: Implications for geocryology
1104 and climate-change science. Permafrost Periglacial Processes 16:5–17
1105 Shmakin AB (2010) Climatic characteristics of snow cover over North Eurasia and their
1106 change during the last decades. Ice and Snow 1:43–57
1107 Skryabin PN, Varlamov SP, Skachkov YB, (2008) Evaluation of recent changes in the
1108 ground thermal state, central Yakutia. In: Proceedings of the Ninth International
1109 Conference on Permafrost. Edited by Kane DL and Hinkel KM. Fairbanks. Institute of
1110 Northern Engineering, University of Alaska Fairbanks, June 29–July 3, Fairbanks,
1111 Alaska, Vol. 2, pp. 1653–1657
1112 Skryabin PN, Varlamov SP (2012) The impact of development and fire on the thermal
1113 state of permafrost, Central Yakutia. TICOP, Vol. 2, 411–414
1114 Smith SL, Wolfe SA, Riseborough DW, Nixon FM (2009) Active-layer characteristics
1115 and summer climatic indices, Mackenzie Valley, Northwest Territories, Canada. Permaf
1116 Periglac Process 20:201–220
1117 Smith SL, Romanovsky VE, Lewkowics AG, Burn CR, Allard M, Clow GD, Yoshikawa
1118 K, Throop J (2010) Thermal state of permafrost in North America: A contribution to the
1119 International Polar Year. Permaf Periglac Process 21:117–135. doi:10.1002/ppp.690
1120 Stieglitz M, Dery SJ, Romanovsky VE, Osterkamp TE (2003) The role of snow cover in
1121 the warming of Arctic permafrost. Geophys Res Lett 30(13):1721.
1122 doi:10.1029/2003GL017337
1123 Strauss J, Schirrmeister L, Grosse G, Wetterich S, Ulrich M, Herzschuh U, Hubberten
1124 H-W (2013) The deep permafrost carbon pool of the Yedoma region in Siberia and
1125 Alaska. Geophys Res Lett 40:1–6. doi:10.1002/2013GL058088
1126 Stroeve JC, Serreze MC, Barrett A, Kindig DN (2011) Attribution of recent changes in
1127 autumn cyclone associated precipitation in the Arctic. Tellus A 63:1–11
1128 Sturm M, Johnson J (1992) Thermal conductivity measurements of depth hoar. J
1129 Geophys Res 97(B2):2129–2139. doi:10.1029/91JB02685
1130 Sturm M, Holmgren J, Liston GE (1995) A seasonal snow cover classification system
1131 for local to global applications. J Clim 8:1261–1283.
1132 doi:10.1175/1520-0442(1995)008<1261:ASSCCS>2.0.CO;2

1133 Takala M, Pulliainen J, Metsämäki S, Koskinen J (2009) Detection of snowmelt using
1134 spaceborne microwave radiometer data in Eurasia from 1979 to 2007. IEEE Trans
1135 Geosci Remote Sensing 47(9): 2996–3007
1136 Tarnocai C, Canadell JG, Schuur EAG, Kuhry P, Mazhitova G, Zimov S (2009) Soil
1137 organic carbon pools in the northern circumpolar permafrost region. Global
1138 Biogeochem Cycles 23:GB2013. doi:10.1029/2008GB003327
1139 Thornton P, Rosenbloom N (2005) Ecosystem model spin-up: Estimating steady state
1140 conditions in a coupled terrestrial carbon and nitrogen cycle model. Ecol Model
1141 189:25–48. Doi:10.1016/j.ecolmodel.2005.04.008
1142 Vasiliev AA, Drozdov DS, Moskalenko NG (2008) The dynamics of permafrost
1143 temperature in West Siberia on context of climate change. Earth Cryosphere
1144 12(2):10–18 (in Russian)
1145 Weedon GP, Gomes S, Viterbo P, Shuttleworth WJ, Blyth E, Österle H, Adam JC,
1146 Bellouin N, Boucher O, Best M (2011) Creation of the WATCH forcing data and its use
1147 to assess global and regional reference crop evaporation over land during the twentieth
1148 century. J Hydrometeor 12:823–848. doi:10.1175/2011JHM1369.1
1149 Zhang T (2005) Influence of the seasonal snow cover on the ground thermal regime: an
1150 overview. Rev Geophys 43:RG4002. doi:10.1029/2004RG000157
1151 Zhang T, Osterkamp TE (1993) Changing climate and permafrost temperatures in the
1152 Alaskan Arctic, in Proceedings of the 6th International Conference on Permafrost,
1153 Beijing, China, July 5–9, 1993, vol. 1, pp. 783–788, S. China Univ. of Pechnol. Press,
1154 Guangzhou, China
1155 Zhang T, Osterkamp TE, Stamnes K (1996) Influence of the depth hoar layer of the
1156 seasonal snow cover on the ground thermal regime. Water Resour Res 32:2075–2086
1157 Zhang T, Stamnes K (1998) Impact of climatic factors on the active layer and
1158 permafrost at Barrow, Alaska. Permaf Periglac Process 9:229–246
1159 Zhang T, Barry RG, Gilichinsky D, Bykhovets SS, Sorokovikov VA, Ye J (2001) An
1160 amplified signal of climatic change in soil temperatures during the last century at
1161 Irkutsk, Russia. Clim Change 49:41–76
1162 Zhang T, Frauenfeld OW, Serreze MC, Etringer A, Oelke C, McCreight J, Barry RG,
1163 Gilichinsk D, Yang D, Ye H, Ling F, Chudinova S (2005) Spatial and temporal
1164 variability in active layer thickness over the Russian Arctic drainage basin. J Geophys
1165 Res 110:D16101. doi:10.1029/2004JD005642

1166 Zhang Y, Chen W, Riseborough DW (2006) Temporal and spatial changes of permafrost
1167 in Canada since the end of the Little Ice Age. J Geophys Res 111:D22103.
1168 Doi:10.1029/2006JD007284
1169 Zhang X, He J, Zhang J, Polyakov I, Gerdes R, Inoue J, Wu P (2013) Enhanced
1170 poleward moisture transport and amplified northern high-latitude wetting trend. Nature
1171 Clim Change 3(1):47–51. doi:10.1038/nclimate1631
1172 Zheleznyak MN (2011) Geocryological Database for the Siberian Platform. In
1173 Proceedings by the All-Russia Conference on Mountain Relief and Exogenenous
1174 Processes. Publishing House of Institute for Geology SB RAS, Irkutsk, pp. 100-103
1175 Zhong X, Zhang T, Wang K (2014) Snow density climatology across the former USSR
1176 8:785–799. Doi:10.5194/tc-8-785-2014
1177

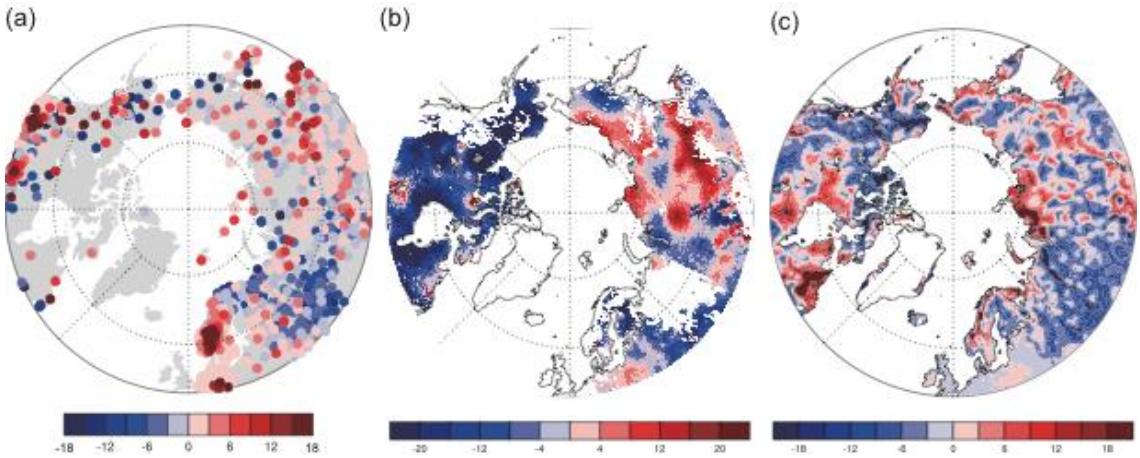

Figure 1. Comparison of decadal anomalies of (a) observed mean winter (DJF) snow depth (cm), (b) mean winter snow water equivalent (mm) provided by GlobSnow based on satellite observations, and (c) simulated mean winter snow depth (cm). The anomalies represent differences in 2001–2009 relative to 1991–2000.

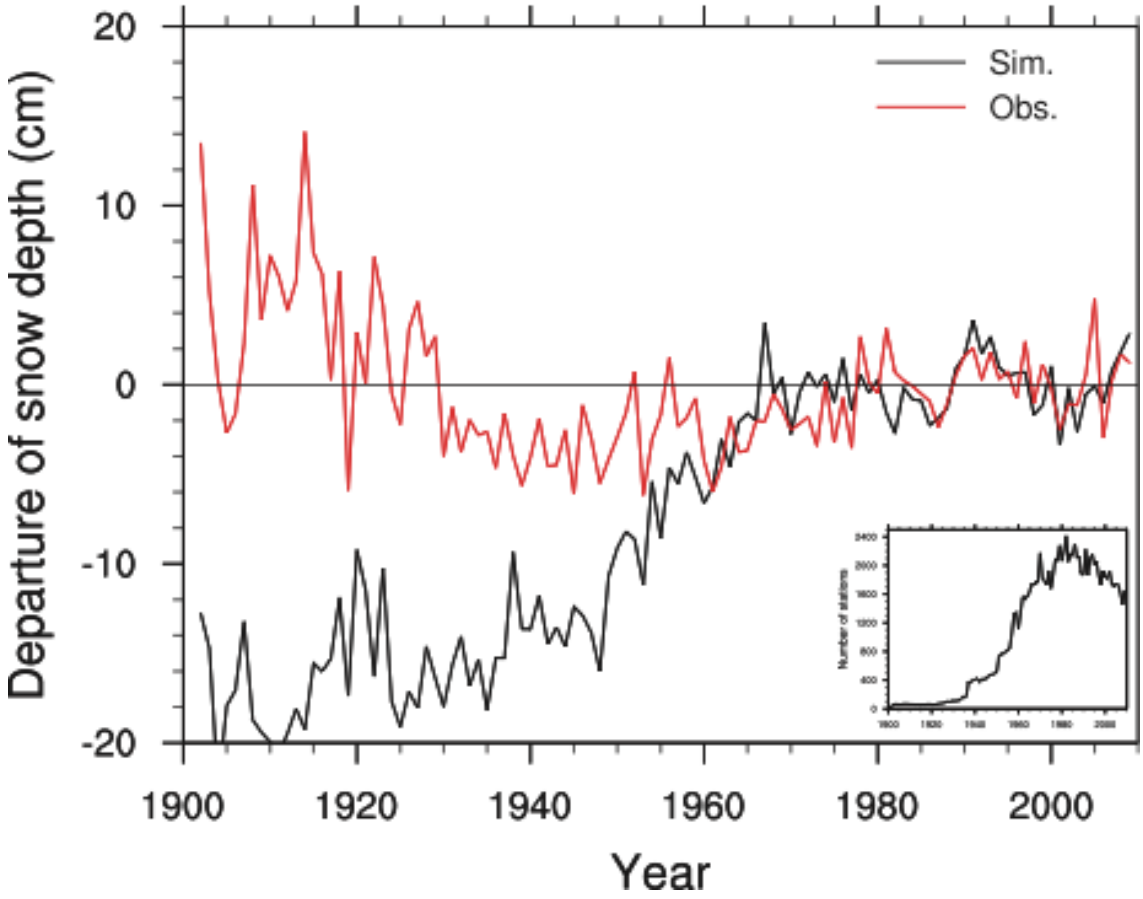

Figure 2. Comparison of interannual anomalies between observed and simulated winter snow depths at the pan-Arctic scale. The anomalies are reduced relative to the averaged values from 1971 to 2000. The inner graph represents the inter-annual variability in the number of stations.

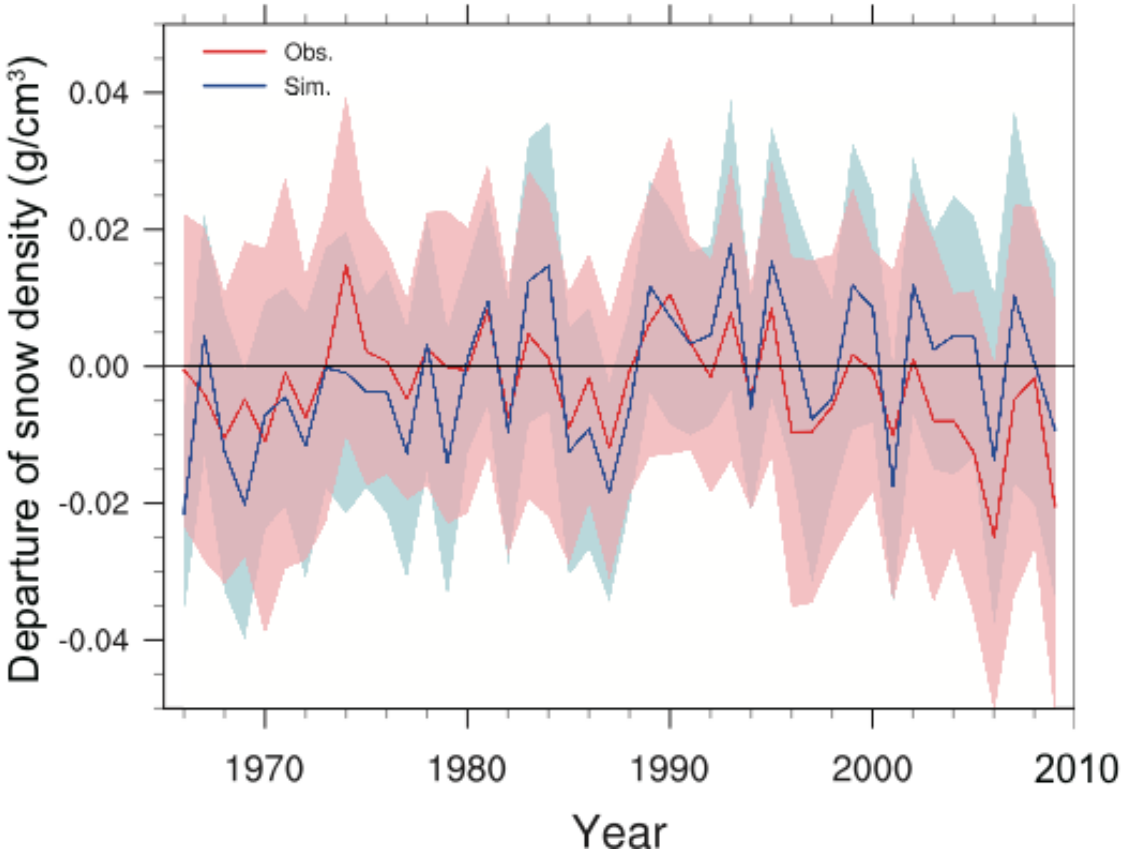

Figure 3. Comparison between observations and simulations in variations of mean snow density in winter (January–March), over a Russian subregion (55°N–70°N, 40°E–140°E) across the former USSR from 1966 through 2009, with respect to the 1971–2000 mean. The shaded areas represent individual one standard deviations from the 1966–2009 mean for each year.

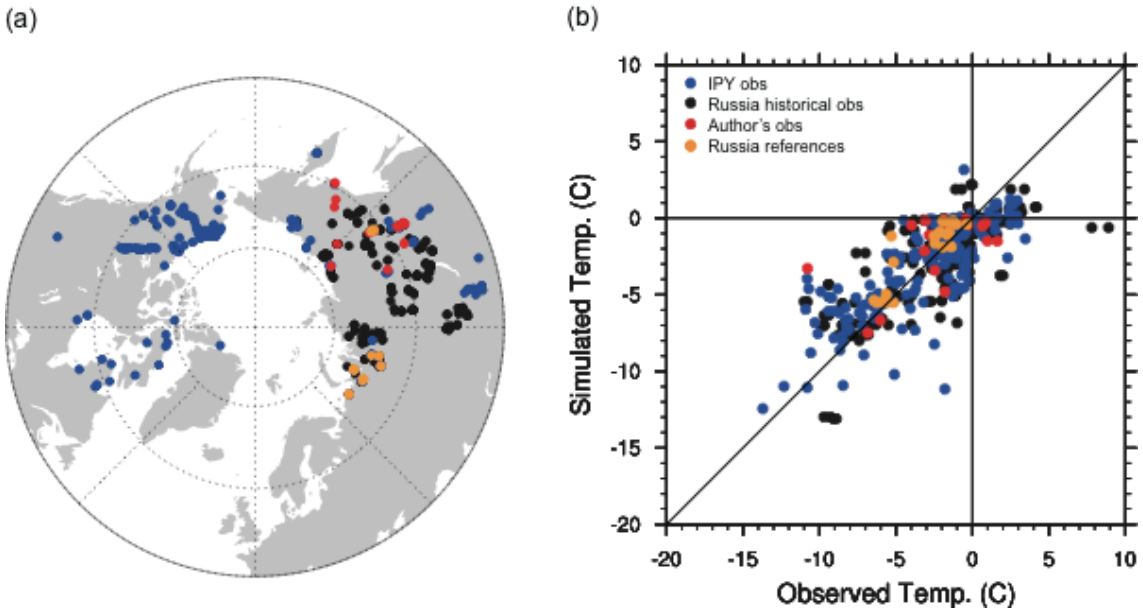

Figure 4. (a) Comparison between borehole observations and simulated temperatures at depths deeper than 10 m and (b) a map showing the locations of borehole sites used for the comparison.

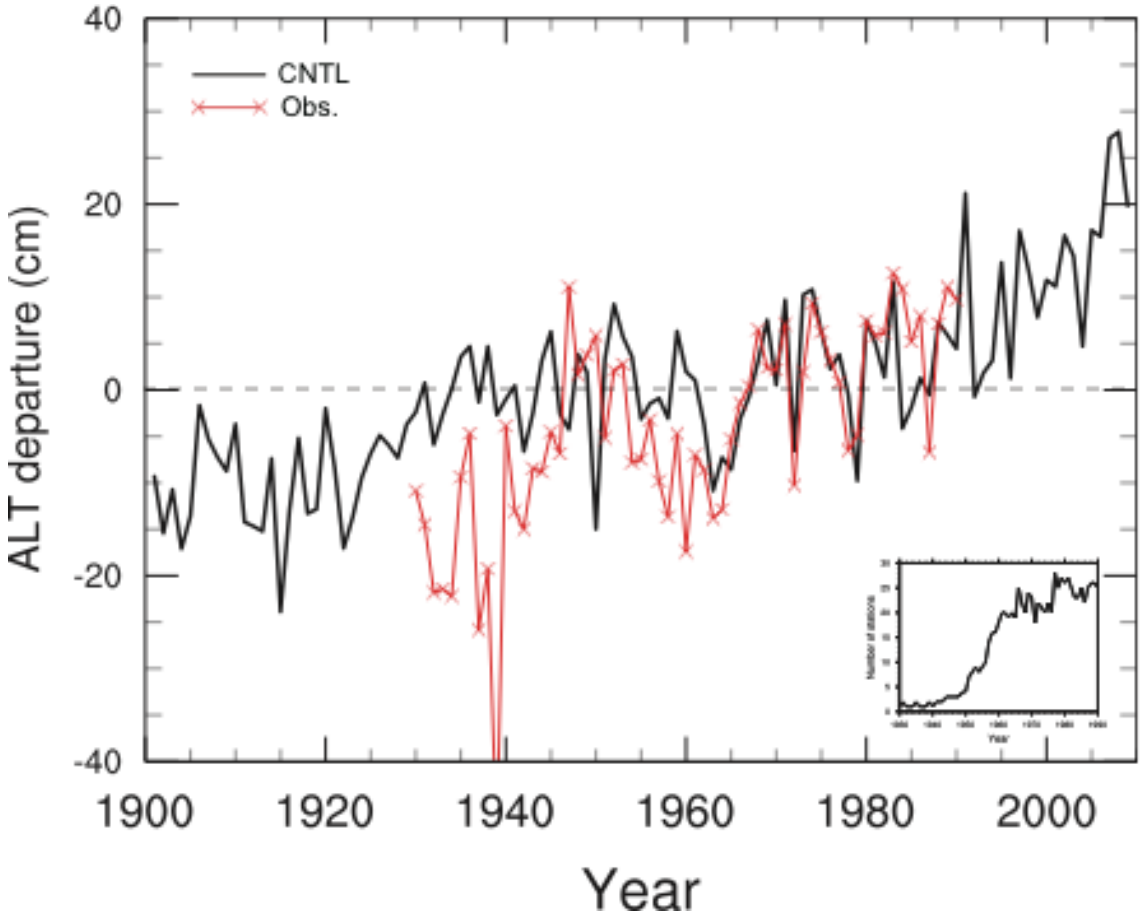

Figure 5. Comparison of interannual variability between simulated and observed active layer thicknesses in eastern Siberia (60ºN–70ºN, 115ºE–165ºE). The observations were derived from soil temperatures observed at 34 Russian meteorological stations. The inner graph represents the interannual variability in the number of stations.

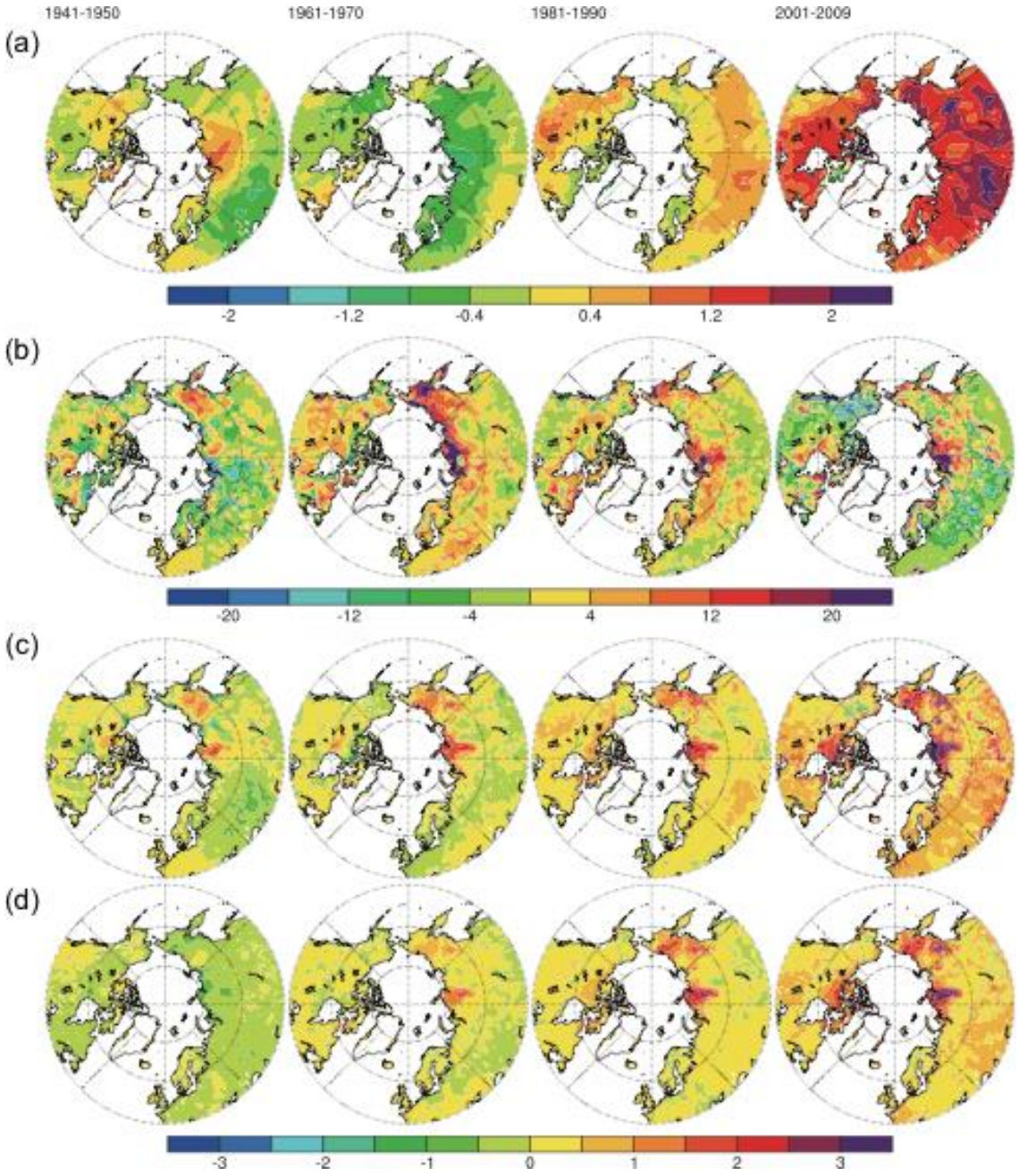

Figure 6. Decadal anomalies of (a) annually averaged surface air temperature (ºC), (b) simulated mean winter (DJF) snow depth (cm), and simulated mean soil temperatures at depths of (c) 3.6 m and (d) 20.4 m (ºC). The decadal anomalies are reduced relative to the averaged values from 1901 to 2009.

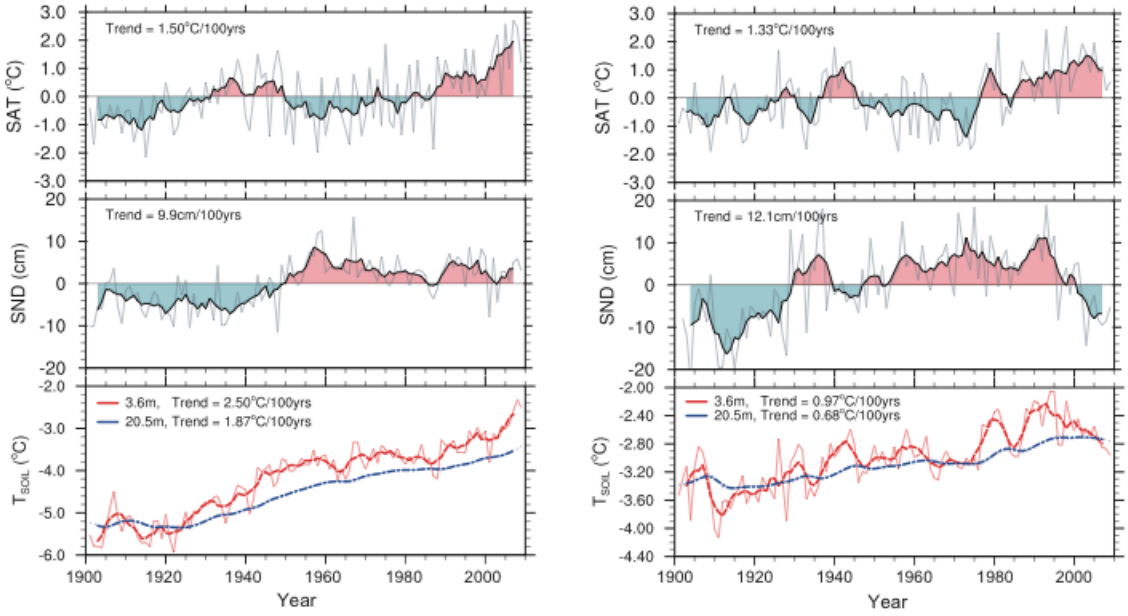

Figure 7. Time series of annual mean surface air temperature (top), simulated winter mean snow depth (middle), and simulated soil temperatures (bottom) at depths of 3.6 m and 20.4 m in Siberia (60ºN–70ºN, 100ºE–140ºE; left) and North America (60ºN–70ºN, 120ºW–160ºW; right).

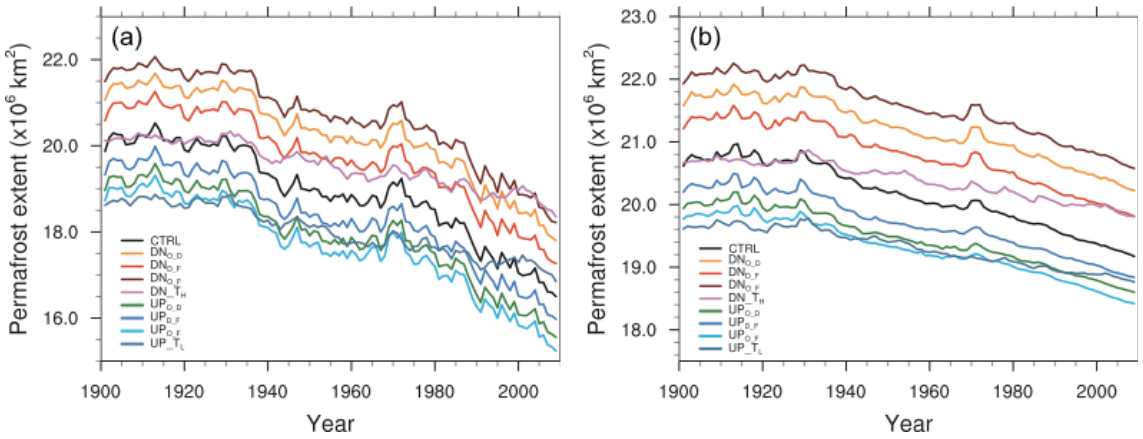

Figure 8. Historical projections of the extent of near-surface permafrost for individual experiments in two cases of the bottom boundary, (a) 3.6 m and (b) 50.5 m. Here, the extent of permafrost represents an integrated area of permafrost in the pan-Arctic region, poleward of 45ºN from the upper part of each bottom boundary.

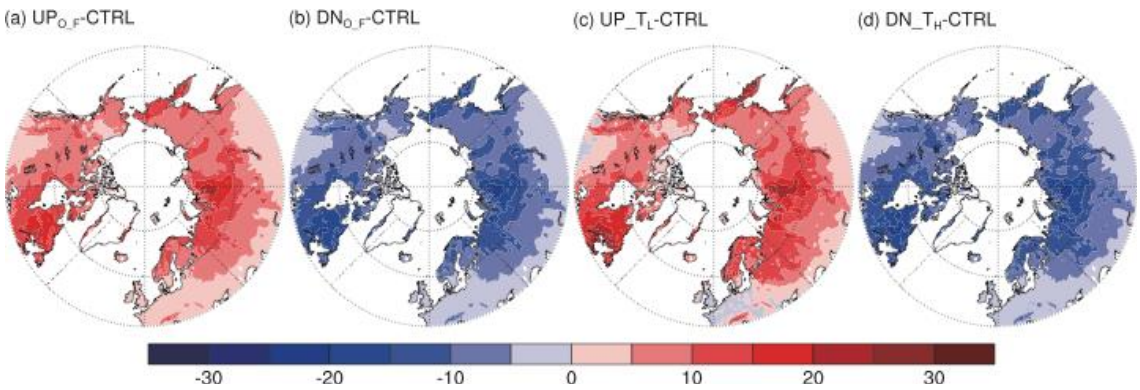

Figure 9. Differences in averaged winter snow depth of (a) UP_{O_F}, (b) DN_{O_F}, (c) UP_T_L, and (d) DN_T_H against the control experiment (CTRL). The mean values were derived during 1981–2009. UP_{O_F}: precipitation was increased by 30% from the amounts projected in the CTRL during October–February, DN_{O_F}: precipitation was decreased by 30% from the amounts projected in the CTRL during October–February, UP_T_L: monthly air temperatures were held at 1911–1930 climatological levels with the treatment of UP_{O_F} for precipitation, DN_T_H: monthly air temperatures were held at 1991–2009 climatological levels with the treatment of DN_{O_F} for precipitation.

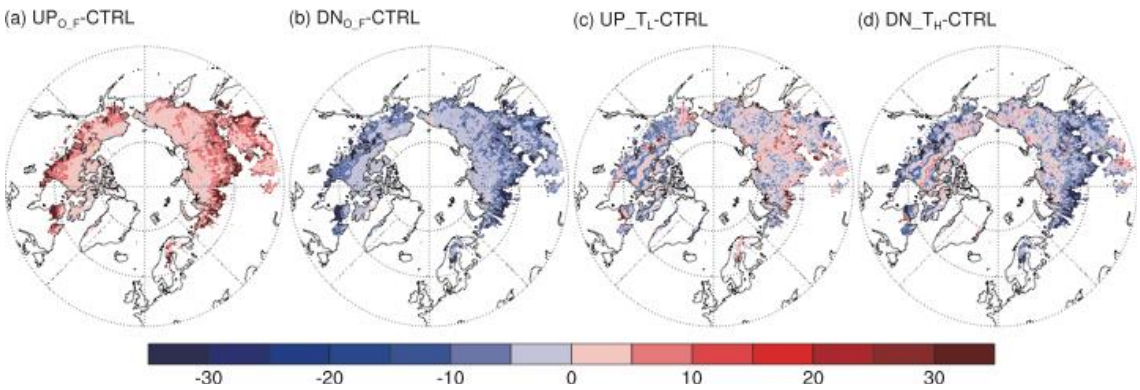

1237

1238 Figure 10. Differences in the maximum active layer thickness of (a) UP_{O_F}, (b) DN_{O_F},
1239 (c) UP_T_L, and (d) DN_T_H against the control experiment (CTRL), averaged during the
1240 period 1981–2009. UP_{O_F}: precipitation was increased by 30% from the amounts
1241 projected in the CTRL during October–February, DN_{O_F}: precipitation was decreased by
1242 30% from the amounts projected in the CTRL during October–February, UP_T_L:
1243 monthly air temperatures were held at 1911–1930 climatological levels with the
1244 treatment of UP_{O_F} for precipitation, DN_T_H: monthly air temperatures were held at
1245 1991–2009 climatological levels with the treatment of DN_{O_F} for precipitation.

1246

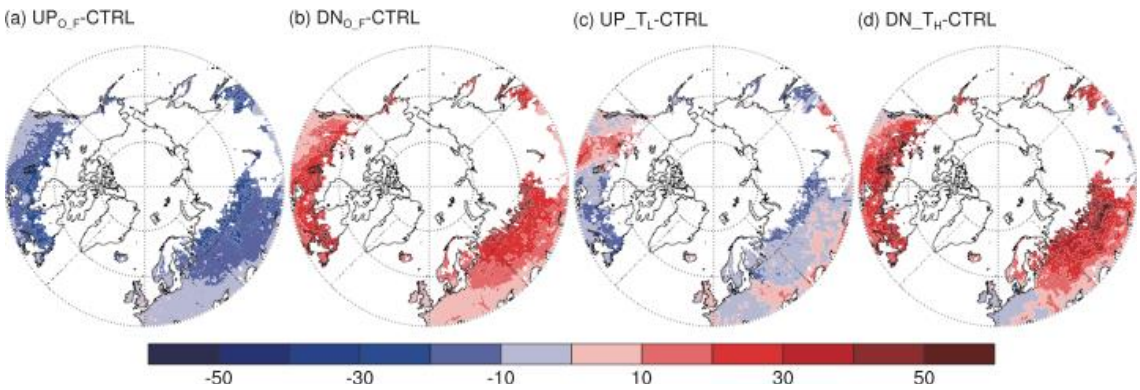

Figure 11. Differences in the maximum freezing thickness of (a) UP_{O_F}, (b) DN_{O_F}, (c) UP_T_L, and (d) DN_T_H against the control experiment (CTRL), averaged during the period 1981–2009. UP_{O_F}: precipitation was increased by 30% from the amounts projected in the CTRL during October–February, DN_{O_F}: precipitation was decreased by 30% from the amounts projected in the CTRL during October–February, UP_T_L: monthly air temperatures were held at 1911–1930 climatological levels with the treatment of UP_{O_F} for precipitation, DN_T_H: monthly air temperatures were held at 1991–2009 climatological levels with the treatment of DN_{O_F} for precipitation.

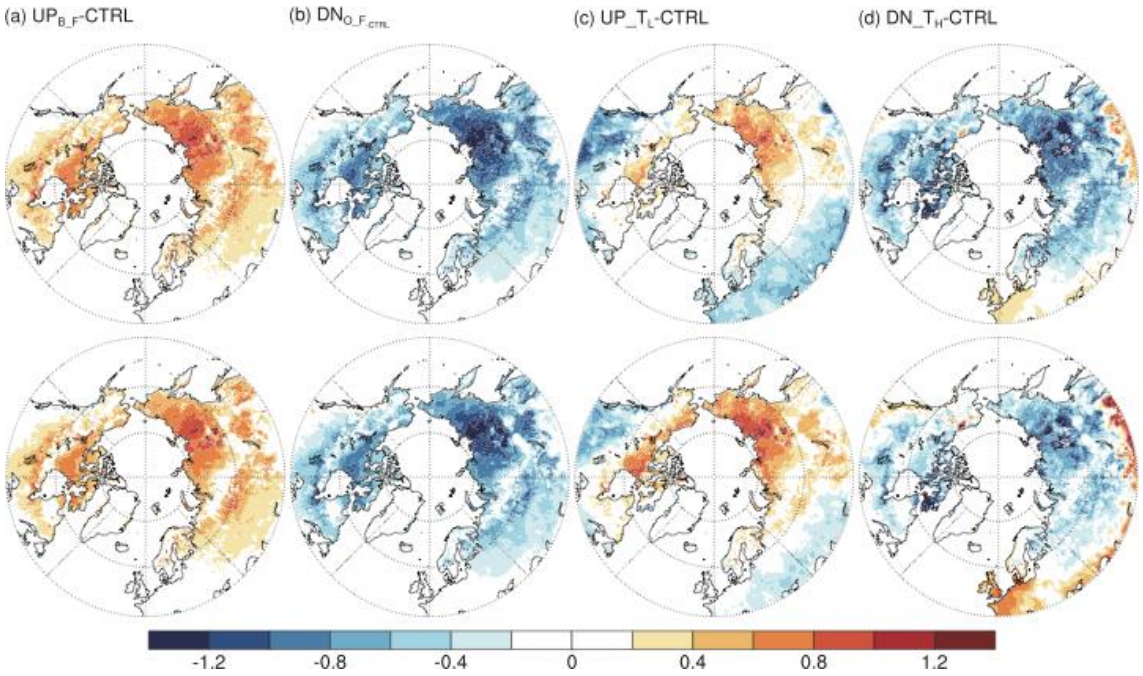

Figure 12. Differences in the averaged soil temperature of (a) UP_{O_F}, (b) DN_{O_F}, (c) UP_T_L, and (d) DN_T_H against the control experiment (CTRL) at depths of 3.6 m (top) and 20.4 m (bottom). The values represent differences derived from 1981–2009. UP_{O_F}: precipitation was increased by 30% from the amounts projected in the CTRL during October–February, DN_{O_F}: precipitation was decreased by 30% from the amounts projected in the CTRL during October–February, UP_T_L: monthly air temperatures were held at 1911–1930 climatological levels with the treatment of UP_{O_F} for precipitation, DN_T_H: monthly air temperatures were held at 1991–2009 climatological levels with the treatment of DN_{O_F} for precipitation.

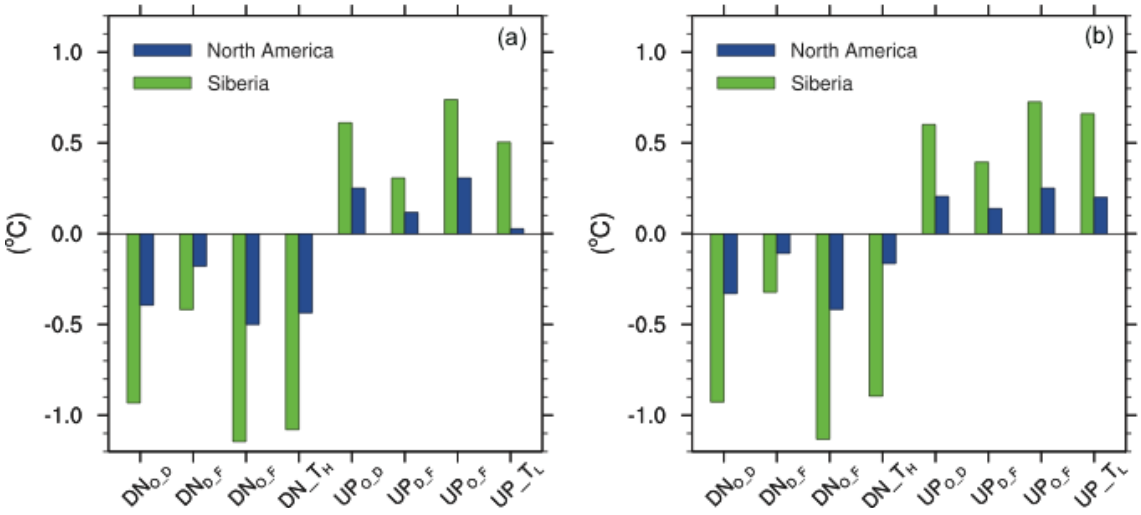

Figure 13. Differences in soil temperatures of individual experiments against the CTRL in northeastern Siberia and North America, defined in Figure 7, during 1981–2009, based on Figure 12. The left panel is for a depth of (a) 3.6 m and the right is for a depth of (b) 20.4 m.

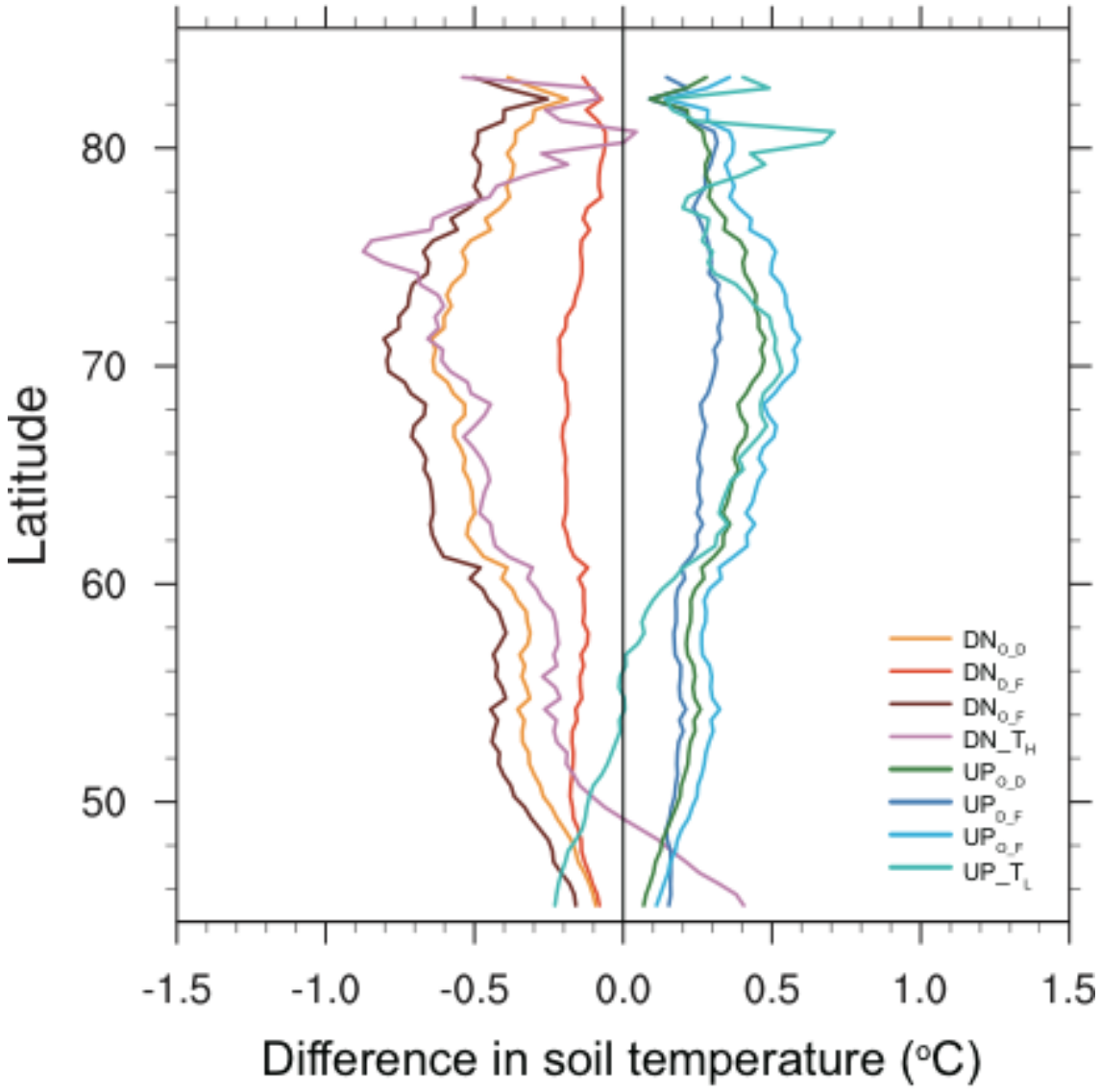

1274

1275 Figure 14. Zonal-averaged profiles of differences in soil temperature at a depth of 20.4
1276 m for individual experiments against control experiment. Profiles were derived based on
1277 Figure 12.

1278

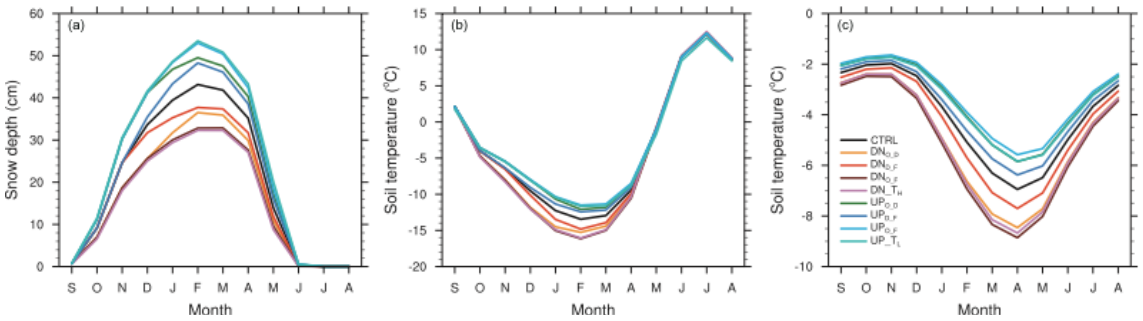

Figure 15. The climatological annual cycles of (a) simulated winter snow depth and (b) the simulated temperatures at the soil surface and (c) a depth of 3.6 m for individual experiments in northeastern Siberia (60ºN–70ºN, 100ºE–140ºE).

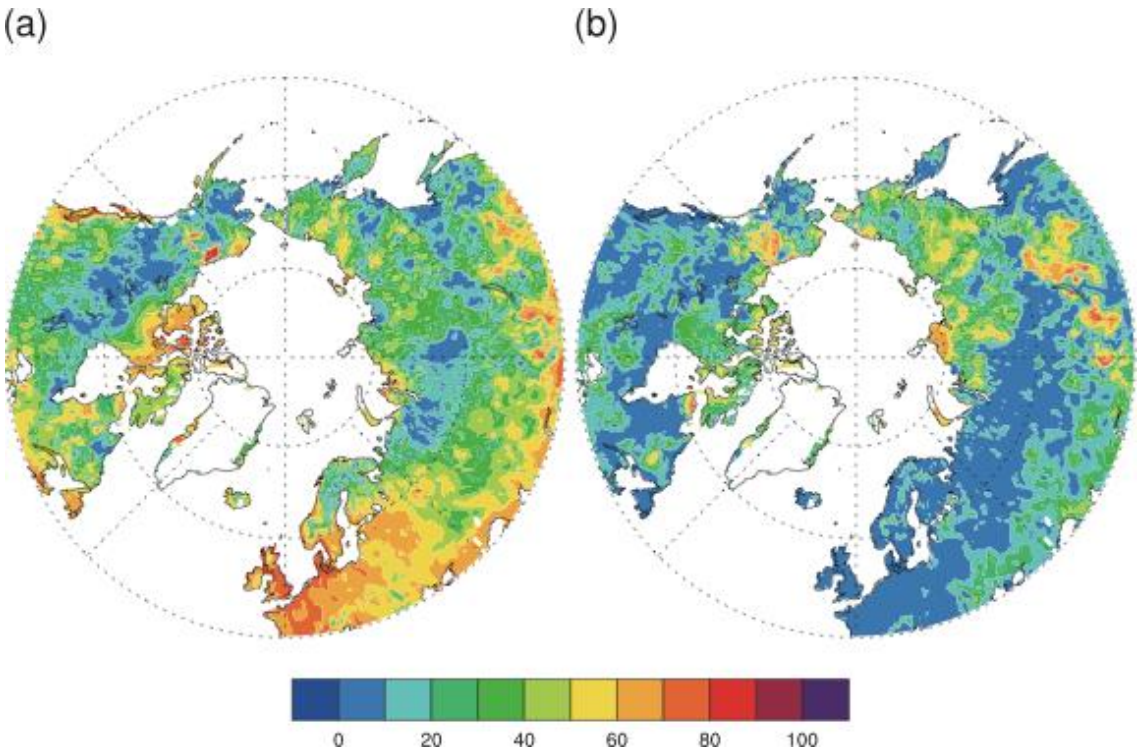

Figure 16. The contribution of (a) annual mean surface temperature and (b) simulated winter snow depth to changes in soil temperature at a depth of 3.6 m during the period 1971–2009.

Table 1. Summary of the model experiments discussed in this study

Name	Description of treatment	
	Air temperature	Precipitation
CTRL	–	–
UP_{O_D}	–	30% added to precipitation from October to December
UP_{D_F}	–	30% added to precipitation from December to February
UP_{O_F}	–	30% added to precipitation from October to February
UP_T_L	Monthly air temperature held at 1911–1930 climatological levels	30% added to precipitation from October to February
DN_{O_D}	–	30% subtracted from precipitation from October to December
DN_{D_F}	–	30% subtracted from precipitation from December to February
DN_{O_F}	–	30% subtracted from precipitation from October to February
DN_T_H	Monthly air temperature held at 1991–2009 climatological levels	30% subtracted from precipitation from October to February

Table 2. Total near-surface permafrost area ($\times 10^6$ km^2) in the Northern Hemisphere (>45°N) during 2001–2009, including previous results. The percentages in the difference represent the increasing rates in permafrost extent of 50.5 m to 3.6 m.

Name	Mean permafrost extent		Difference
	3.6 m	50.5 m	(= 50.5 m – 3.6 m)
Observed	12.2–17.0*		
CTRL	16.8	19.3	2.5 (14.9%)
DN_{O_D}	18.2	20.3	2.1 (11.5%)
DN_{D_F}	17.6	19.9	2.3 (13.1%)
DN_{O_F}	18.6	20.7	2.1 (11.3%)
DN_T_H	18.7	19.9	1.2 (6.4%)
UP_{O_D}	15.9	18.7	2.8 (17.6%)
UP_{D_F}	16.3	18.9	2.6 (16.0%)
UP_{O_F}	15.6	18.5	2.9 (18.6%)
UP_T_L	17.2	18.8	1.6 (9.3%)
CCSM	11.1–13.7†		
JULES	12.2–15.7††		

* Zhang et al. (2003)

†Lawrence et al. (2012) adopted the bottom soil boundary less than 3.8 m.

††Burke et al. (2013) considered the bottom soil boundary less than 7 m, in which the result of an experiment with zero snow layer is excluded.